ecologies

MDPI

Article

Patterns of Plant Biodiversity Recovery in Post-Fire Rehabilitation Microsites: A Two-Year Study in Ancient Olympia (Greece)

Alexandra D. Solomou [1,*], Nikolaos Proutsos [1], Panagiotis Michopoulos [1], Athanassios Bourletsikas [1] and Panagiotis Lattas [2]

1 Institute of Mediterranean Forest Ecosystems (IMFE), Hellenic Agricultural Organization-DIMITRA, Terma Alkmanos, Ilisia, 11528 Athens, Greece; nproutsos@elgo.gr (N.P.); pmichopoulos@elgo.gr (P.M.); abourletsikas@elgo.gr (A.B.)
2 Forest Department of Pyrgos, Forests Directorate General of Ilia, 42 Alfiou, 21731 Pyrgos, Greece; p.lattas@eedpdpi.ypen.gr
* Correspondence: asolomou@elgo.gr

Abstract

Post-fire rehabilitation structures are widely used in Mediterranean burned landscapes to reduce runoff and sediment transfer, yet their ecological associations with early vegetation recovery remain insufficiently documented. This observational study assessed vascular plant composition, species richness, vegetation cover, plant density, aboveground biomass, and soil properties across log barriers, wattles, and log dams in the burned landscape of Ancient Olympia, western Greece. The study area belongs to the humid climatic class of the United Nations Environment Programme (UNEP) aridity framework based on the Thornthwaite aridity index, providing a comparatively wetter Mediterranean post-fire context. Paired depositional and eroded microsites in operationally restored post-fire areas were monitored in 2022 and 2023. The sampling design comprised nine plots and 18 microsites (n = 9 plots, 18 microsites). Generalized estimating equations (GEE), change-score models, principal component analysis (PCA) and permutational multivariate analysis of variance (PERMANOVA) were performed to examine associations of monitoring year, microsite condition and rehabilitation structure type with soil and vegetation patterns. A total of 27 vascular plant species belonging to 16 families were recorded. The average vegetation cover increased from 39.17 $\pm$ 21.44% in 2022 to 75.11 $\pm$ 12.90% in 2023. Model-based marginal estimates with 95% confidence intervals indicated a large positive increase in vegetation cover over this period. Further, rapid early recovery was indicated by large increases in species richness, plant density and biomass. Depositional microsites were associated with stronger recovery signals than eroded ones, characterized by a larger increase in vegetation cover, density, biomass and species richness. Among rehabilitation structures, log dams showed the highest cumulative floristic richness and a broader observed floristic spectrum, although the species-level contingency analysis provided only marginal evidence for structure-associated differences in floristic composition. Changes in selected soil properties including total nitrogen (total N), ammonium nitrogen (NH4-N), nitrate nitrogen (NO3-N), pH, electrical conductivity (EC), and exchangeable calcium (Ca), magnesium (Mg), and potassium (K), were detected between 2022 and 2023; the multivariate soil pattern was driven primarily by mineral nitrogen, pH, and EC. These findings suggest that, under operational post-fire restoration conditions, rehabilitation structures are associated not only with erosion-control functions but also with microsite differentiation that may shape early plant establishment and biodiversity recovery in Mediterranean burned landscapes.

Academic Editor: Giorgos Kokkoris

Received: 5 May 2026
Revised: 14 June 2026
Accepted: 18 June 2026
Published: 22 June 2026

Keywords: vascular plants; species richness; log barriers; wattles; log dams; soil properties; erosion-control structures; depositional zones; eroded zones; Mediterranean burned landscapes

1. Introduction

Wildfire is a recurrent ecological disturbance in Mediterranean-type ecosystems, where vegetation dynamics, soil properties and hydrological processes are closely coupled. More recent evidence indicates that extreme wildfire activity and fire-weather extremes have intensified in recent decades: the frequency of the most energetically extreme wildfire events increased 2.2-fold from 2003 to 2023, while European fire-weather extremes have become more frequent, affected increasingly larger areas, and occurred earlier and later in the fire season [1,2]. Climate-projection analyses also indicate that warming could substantially increase the probability of extreme fire events in southern Europe [3]. In the immediate post-fire period, the loss of vegetation cover and litter, ash redistribution and fire-induced changes in soil physical and chemical properties can increase runoff generation, sediment detachment, nutrient redistribution and erosion risk, particularly on steep slopes [4–7]. Because this early post-fire window is often the period of greatest geomorphological sensitivity, emergency rehabilitation commonly aims to reduce runoff connectivity, retain sediment and protect recovering soils before vegetation cover is re-established [5,8].

Nature-based wooden structures, including contour log barriers, wattles or brush structures, and log dams, are widely used for post-fire stabilization, often using locally available burned wood and branches [8–13]. Their performance has traditionally been evaluated through physical and hydrological criteria, such as runoff attenuation, infiltration enhancement and sediment retention. Meta-analytical and field-based evidence indicates that barrier and cover-based treatments can reduce post-fire soil erosion, although their effectiveness is strongly context-dependent and varies with rainfall regime, slope, burn severity, soil properties, installation quality and sediment-storage capacity [8,11–13].

However, post-fire rehabilitation success cannot be assessed only through engineering or hydrological indicators. Vegetation recovery is a central component of ecosystem resilience because increasing plant cover, biomass and root development contribute to long-term slope stabilization, nutrient cycling, habitat reassembly and biodiversity conservation [14–17]. In Mediterranean fire-prone ecosystems, early vegetation recovery is shaped by regeneration strategies, especially the balance between resprouting and post-fire seedling recruitment, as well as by drought stress, soil conditions and microsite availability [15,18–20]. Therefore, post-fire interventions may influence ecological recovery when they modify the small-scale conditions under which propagules are trapped, seedlings establish and surviving plants resprout.

Wooden rehabilitation structures may therefore act not only as erosion-control devices but also as microsite-forming ecological filters. By increasing surface roughness and creating depositional zones, these structures can affect sediment and litter accumulation, shading, near-surface moisture, nutrient redistribution and propagule retention. Such effects may generate contrasts between depositional microsites immediately upslope of structures and more eroded microsites located between consecutive structures [8,10]. Despite this potential ecological role, comparative vegetation-based assessments among operational rehabilitation structure types remain limited, particularly in Greece, where log barriers, wattles and log dams are frequently implemented after wildfire but have been evaluated mainly through erosion-control, hydrological or soil-related indicators [9,10,21]. The technical report by

Proutsos et al. [9] is a project deliverable/final technical report of the MOnitoring the impact of REstoration works in the post-fire forest environment in Greece (MoRe Forests) project and is cited here only for project-specific information on the operational implementation of post-fire rehabilitation works, site selection, and monitoring context, not as peer-reviewed evidence. A recently published two-year study from Greece provides complementary evidence on vascular plant biodiversity and indicator-species responses across post-fire rehabilitation structures [21].

Ancient Olympia, western Greece, provides an informative case study for assessing these processes under operational post-fire rehabilitation conditions. The area was affected by a large wildfire in August 2021, after which rehabilitation works were implemented using log barriers, wattles and log dams [7,9]. The broader Pothos area also belongs to the humid climatic class of the UNEP aridity framework, based on the Thornthwaite aridity index, contrasting with more semi-arid Greek post-fire study areas [22–26]. This climatic context allows the evaluation of whether common wooden rehabilitation structures are associated with differentiated early vegetation recovery under comparatively wetter Mediterranean conditions.

The aim of this study was to assess early post-fire vegetation recovery and plant diversity across three common rehabilitation structures, namely log barriers, wattles and log dams, in the burned landscape of Ancient Olympia. Specifically, we compared vascular plant composition, species richness, vegetation cover, plant density, aboveground biomass and soil properties between depositional and eroded microsites during the first two post-fire monitoring years, 2022 and 2023. It was hypothesized that depositional microsites would support stronger vegetation recovery than eroded microsites because they are expected to retain more sediment, organic material, propagules and near-surface moisture. It was further hypothesized that vegetation and soil recovery patterns would differ among rehabilitation structure types, because log barriers, wattles, and log dams differ in their geomorphic position, sediment-retention function, and capacity to modify local microsite conditions. By integrating floristic, structural vegetation and soil indicators at the microsite scale, this study addresses an important gap in post-fire rehabilitation assessment: whether operational erosion-control structures also contribute to early biodiversity recovery and ecosystem resilience in Mediterranean burned landscapes.

2. Materials and Methods

2.1. Study Site

The study was carried out in the Pothos site of the burned landscape of Ancient Olympia, in the Regional Unit of Ilia, Western Greece. Administratively, the area falls under the jurisdiction of the Forest Directorate of Ilia and the Pyrgos Forest Service [9]. The broader landscape was affected by the major wildfire of 4 August 2021, for which the Copernicus Emergency Management Service was activated, and the project technical documentation estimated a burned area of approximately 18,135 ha [9,22]. Site location is provided with geographic coordinates and elevation, and the timing and extent of the 2021 fire events are documented in official fire-recording platforms and associated reporting sources (Table 1).

Table 1. Geographical, topographic, and geological characteristics of the study plots and types of rehabilitation structures for the study area.

Site	Plot	Longitude, Degrees (Deg.)	Longitude, Minutes (min)	Latitude, Degrees (Deg.)	Latitude, Minutes (min)	Altitude, Metres (m)	Slope, Degrees (Deg.)	Aspect, Degrees (Deg.)	Structure Type	Parental Rock
Pothos	PTH01	21	41.4709	37	42.3249	719	38	234	log barrier	Tertiary deposits
Pothos	PTH02	21	41.5233	37	42.3032	709	34	253	log barrier	Tertiary deposits
Pothos	PTH03	21	41.4797	37	42.3208	703	37	195	log barrier	Tertiary deposits
Pothos	PTH04	21	41.4789	37	42.2936	712	15	200	wattle	Tertiary deposits
Pothos	PTH05	21	41.4755	37	42.2920	712	15	198	wattle	Tertiary deposits
Pothos	PTH06	21	41.4770	37	42.2897	709	13	198	wattle	Tertiary deposits
Pothos	PTH07	21	41.4634	37	42.3218	717	32	190	log dam	Tertiary deposits
Pothos	PTH08	21	41.3173	37	42.3212	720	39	174	log dam	Tertiary deposits
Pothos	PTH09	21	41.4613	37	42.3180	721	25	170	log dam	Tertiary deposits

The revised Figure 1 depicts the spatial context of the study region, including Ancient Olympia in Greece, the boundary of the 2021 wildfire, and the sites of the nine experimental plots categorized based on the three rehabilitation structural types: log barriers, wattles, and log dams.

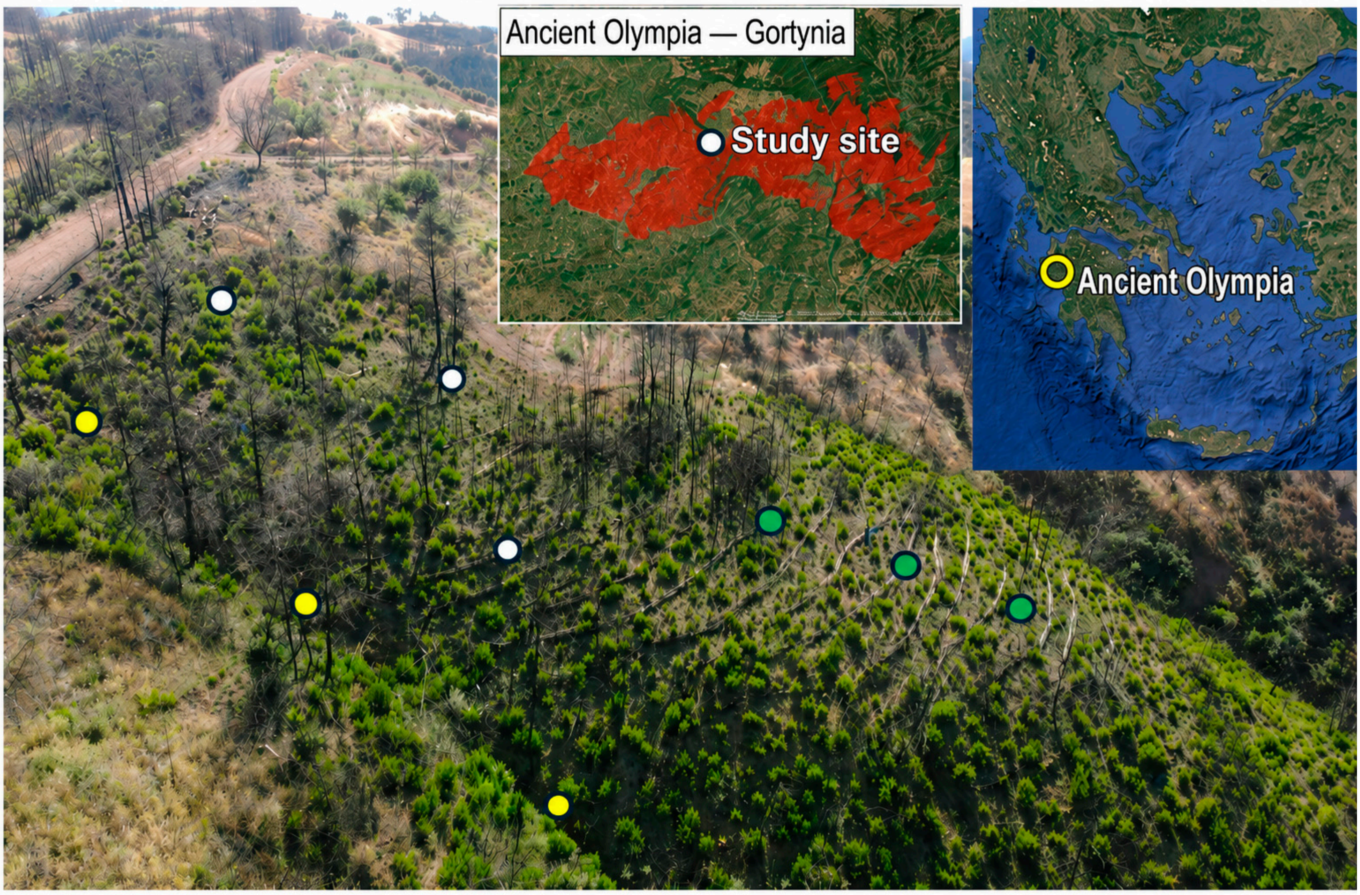

Figure 1. Location of the study area and sampling plots in Ancient Olympia, western Greece. The right inset shows the position of Ancient Olympia within Greece, the upper inset shows the perimeter of the 2021 Ancient Olympia–Gortynia wildfire and the study-site location, and the coloured plot markers indicate the distribution of the nine experimental plots according to rehabilitation structure type: log barriers (white dots), wattles (green dots), and log dams (yellow dots).

The experimental plots were located on sloping terrain, with slope angles ranging from 13° to 39° across the nine plots. Because slopes can affect the generation of runoff, sediment redistribution and the establishment of plants, slopes were included as a covariate in the statistical models.

The soils of the study plots are developed on Tertiary deposits and are described here, following the World Reference Base for Soil Resources (WRB), as Calcaric Cambisols (Loamic) at broad reference-group level. This classification is consistent with the sandy-loam texture reported for nearly all samples, the presence of calcium carbonate, and the neutral to alkaline soil reaction observed in the soil analytical dataset. Because the present study was designed as an operational post-fire monitoring survey and did not include full pedon descriptions or diagnostic-horizon assessment, the WRB classification is reported at reference-group and main-qualifier level rather than as a complete pedon-level qualifier sequence [27]. To provide a clearer background description of the soil environment, the main physical and chemical characteristics of the upper mineral soil are summarized in Table 2. These values describe the topsoil context of the monitored burned plots and provide background information for interpreting the vegetation and soil response patterns reported below. They should not be interpreted as pre-fire baseline values, because no pre-fire soil characterization was available for the monitored plots.

The particle-size distribution of the upper mineral soil showed a clear dominance of the sand fraction. Across the reported structure–microsite combinations, sand ranged from 58.7% to 69.3%, clay from 11.8% to 18.6%, and silt from 18.8% to 24.2%. These values indicate that the background topsoil of the monitored burned plots was predominantly sandy loam (Tables 3 and 4). The relatively high sand content is relevant for interpreting post-fire soil and vegetation responses, because sandy-loam soils generally have lower water-retention capacity than finer-textured soils, while still allowing relatively rapid drainage and infiltration. The particle-size data are reported here as background topsoil characteristics of the monitored burned plots and should not be interpreted as pre-fire baseline values. The comparison between eroded and depositional microsites indicates modest particle-size redistribution at the microsite scale. Because no pre-erosion particle-size baseline was available, these values should be interpreted as spatial contrasts between erosion-affected and depositional microsites rather than as direct temporal changes caused by erosion. Across all rehabilitation structure types, the dominant texture class remained sandy loam. However, eroded microsites generally had higher clay percentages than depositional microsites: 15.3% versus 11.8% in wattles, 18.6% versus 13.9% in log barriers, and 15.8% versus 13.4% in log dams. Sand was lower in eroded than in depositional microsites for all three structure types, with the strongest contrast in wattles. These patterns indicate that erosion-affected microsites were relatively finer-textured, particularly in terms of clay enrichment, whereas depositional microsites tended to contain slightly higher sand percentages. Soil structure or aggregate state was not evaluated as an erosion-response variable, because the analyses were based on disturbed, air-dried, sieved, and homogenized mineral soil samples rather than undisturbed field observations of natural aggregates.

According to long-term climatic data from the nearest Hellenic National Meteorological Service station at Pyrgos, the broader study area belongs to the humid climatic class under the United Nations Environment Programme (UNEP) aridity classification system, which is based on the Thornthwaite aridity index [9,23–26]. More specifically, the aridity index of the area was reported as 1.02 for the recent climatic period 1960–1997, compared with 0.92 for the earlier climatic period 1930–1960 [9,23–26]. This places the study area in a comparatively wetter climatic setting than other recently investigated burned forest landscapes in Greece.

https://doi.org/10.3390/ecologies7020059

Table 2. Background topsoil characteristics of the monitored burned plots.

Soil Characteristic	Unit/Basis	Background Value or Description
Parent material	—	Tertiary deposits
Coarse surface fragments/rock debris	Visual cover class; size class	Natural coarse surface fragments derived from Tertiary deposits; mainly gravel- to stone-sized fragments. In the 1 × 1 m quadrat, visible cover was estimated at approximately 15–40% of the surface. Coarse-fragment cover was not systematically measured across all plots and was not included in the statistical analyses.
Expected effect of coarse surface fragments on erosion	Qualitative interpretation	Likely moderation of water-driven erosion by reducing raindrop detachment, limiting surface sealing, increasing surface roughness, slowing overland flow, and promoting localized sediment retention. Effect not quantified because coarse-fragment cover was not systematically measured across all plots.
World Reference Base for Soil Resources (WRB) classification	—	Calcaric Cambisols (Loamic), reported at broad reference-group and main-qualifier level
Sampling depth	cm	0–20
Humus/surface organic horizon thickness	cm	Not measured separately; loose surface litter, ash, roots, and coarse organic debris were removed before collecting the 0–20 cm mineral soil sample
Dominant texture class	—	Sandy loam
Soil structure/aggregate state	—	Not determined separately; the analytical dataset was based on disturbed 0–20 cm mineral soil samples, so no formal field classification of aggregate structure is reported
Sand	%	58.7–69.3
Clay	%	11.8–18.6
Silt	%	18.8–24.2
Calcium carbonate ($CaCO_3$)	%	0–87; mean approximately 9
Soil reaction, pH	pH units	Neutral to slightly alkaline; initial post-fire mean in the monitoring dataset: 7.31 ± 0.44
Electrical conductivity (EC)	$\mu S\ cm^{-1}$	Initial post-fire mean in the monitoring dataset: 1002.70 ± 622.82
Organic carbon	%	2.80–4.36
Total nitrogen (total N)	$mg\ g^{-1}$	Initial post-fire mean in the monitoring dataset: 2.00 ± 0.72
Carbon to nitrogen ratio (C/N)	—	12.3–16.5
Ammonium nitrogen (NH_4-N)	$mg\ kg^{-1}$	Initial post-fire mean in the monitoring dataset: 13.17 ± 7.17
Nitrate nitrogen (NO_3-N)	$mg\ kg^{-1}$	Initial post-fire mean in the monitoring dataset: 54.16 ± 39.59
Exchangeable calcium (Ca), magnesium (Mg), potassium (K), and sodium (Na)	meq 100 g^{-1} soil	Measured as part of the soil analytical dataset
Soil moisture	%	Measured volumetrically as percentage water content
Predominant erosion process	—	Water-driven post-fire erosion associated with rainfall-runoff and sediment redistribution; wind erosion was not monitored separately

Table note: Values summarize the upper mineral soil of the monitored burned plots and provide soil-background context for interpreting the post-fire vegetation and soil response patterns. They should not be interpreted as pre-fire baseline values, because no pre-fire soil characterization was available for the monitored plots. Particle-size, organic carbon (organic C), carbon-to-nitrogen ratio (C/N), calcium carbonate ($CaCO_3$), and texture information are reported as background ranges from the related soil dataset, whereas pH, electrical conductivity (EC), total nitrogen (total N), ammonium nitrogen (NH_4-N), and nitrate nitrogen (NO_3-N) are shown as initial post-fire mean ± standard deviation (SD) values from the 2022 monitoring dataset. All analytical values are expressed on an air-dry soil basis. Humus or surface organic horizon thickness was not quantified separately; therefore, no numerical thickness is reported for this layer. Soil structure/aggregate state was not classified separately because the analyses were based on disturbed, sieved mineral soil samples rather than undisturbed field pedon descriptions.

https://doi.org/10.3390/ecologies7020059

Table 3. Particle-size distribution and dominant texture class of the upper mineral soil across rehabilitation structure types and microsites.

Structure Type	Microsite	Sand (%)	Clay (%)	Silt (%)	Dominant Texture Class
Wattles	Eroded zone	61.5	15.3	23.2	Sandy loam
Wattles	Deposition zone	69.3	11.8	18.8	Sandy loam
Log barriers	Eroded zone	58.7	18.6	22.7	Sandy loam
Log barriers	Deposition zone	61.9	13.9	24.2	Sandy loam
Log dams	Eroded zone	64.4	15.8	19.8	Sandy loam
Log dams	Deposition zone	65.0	13.4	21.7	Sandy loam

Table note: Particle-size distribution was determined by the hydrometer method and is expressed as percentage sand, clay, and silt on an air-dry soil basis. Values represent mean particle-size percentages for the corresponding structure–microsite combinations and provide background topsoil information for the monitored burned plots.

Table 4. Particle-size contrasts between eroded and depositional microsites in the upper mineral soil.

Structure Type	Sand in Eroded Zone (%)	Sand in Deposition Zone (%)	Δ Sand, Eroded—Deposition	Clay in Eroded Zone (%)	Clay in Deposition Zone (%)	Δ Clay, Eroded—Deposition	Silt in Eroded Zone (%)	Silt in Deposition Zone (%)	Δ Silt, Eroded—Deposition	Interpretation
Wattles	61.5	69.3	−7.8	15.3	11.8	3.5	23.2	18.8	4.4	Eroded zone relatively finer; depositional zone sandier
Log barriers	58.7	61.9	−3.2	18.6	13.9	4.7	22.7	24.2	−1.5	Strongest clay enrichment in eroded zone
Log dams	64.4	65	−0.6	15.8	13.4	2.4	19.8	21.7	−1.9	Small particle-size contrast; same texture class retained

Table note: Positive Δ values indicate higher percentages in eroded microsites than in depositional microsites; negative values indicate lower percentages in eroded microsites. Values represent spatial contrasts between eroded and depositional microsites, not direct temporal changes during erosion. Soil structure/aggregate state was not quantified from undisturbed field observations.

Recent meteorological data from the nearest meteorological station of the National Observatory of Athens in Pyrgos (37°42′ N, 21°24′ E, altitude (Alt): 22 m, www.meteo.gr, accessed on 12 December 2023) indicate similar annual air temperature values both for the wildfire year (2021) and for the subsequent two post-fire years (19.2 °C in 2021 and 2022, and 19.3 °C in 2023). In contrast, the annual precipitation exhibited higher interannual variability with 2021 being much wetter (1145 mm) than 2022 (667 mm) and 2023 (771 mm). A more detailed description of the prevailing meteorological conditions in the broader study area is provided by Proutsos et al. [10].

The site was selected because it fulfilled the main criteria of the national monitoring project: it had burned during the 2021 fire season, post-fire rehabilitation works had been implemented relatively recently, and different types of erosion-control structures co-occurred within the same burned landscape, allowing their comparative evaluation [9]. The present study should therefore be interpreted as an assessment of early post-fire vegetation recovery across rehabilitation structure types within an operationally restored burned area.

2.2. Experimental Plots

In summer 2022, nine experimental plots were established as part of operationally implemented post-fire rehabilitation works in Pothos [9]. The plots were equally distributed among the three locally prevalent structural types, namely log barriers (PTH01–PTH03), wattles (PTH04–PTH06), and log dams (PTH07–PTH09 (Figure 2) [9]. This report draws on Greek rehabilitation practice, where log barriers primarily refer to logs and trunks positioned on a hill slope, wattles are branch-based linear brush structures, and log dams are structural wooden barriers built across a small channel or streambed to slow flow and trap sediment [9,21].

Figure 2. Different types of erosion-control structures: (**a**) log barriers, (**b**) log dams, and (**c**) wattles.

Each plot was defined as the area between two consecutive rehabilitation units, following the monitoring framework adopted in the broader national project [9,21]. Within each plot, two functionally distinct microsites were recognized. The first corresponded to the depositional zone, located immediately upslope of the structure, where transported soil material and organic debris accumulated. The second corresponded to the eroded zone, located approximately midway between two consecutive structures, where sediment removal was more evident [9].

In the experimental plots, the predominant erosion process was considered to be water-driven post-fire erosion, mainly associated with rainfall-runoff, downslope sediment transport, and local sediment deposition. This interpretation is consistent with the position and function of the rehabilitation structures: log barriers and wattles were installed on hillslopes to interrupt overland flow and sediment transfer, whereas log dams were placed in small channels or ephemeral streambeds to slow concentrated flow and retain transported material. Wind erosion was not monitored as a separate process and was not considered the dominant erosion mechanism in this study. Therefore, the terms "eroded zone" and "depositional zone" refer to water-driven sediment removal and accumulation patterns within the monitored post-fire rehabilitation plots.

The study followed an observational monitoring design within operationally implemented post-fire rehabilitation works. Therefore, the structure types were compared under real restoration conditions rather than under a fully randomized experimental treatment design [9,21]. Plot placement was constrained by the actual distribution of log barriers, wattles, and log dams in the field. The absence of untreated burned control plots means that the results should be interpreted as structure- and microsite-associated recovery patterns, not as strict causal estimates of treatment effects. Fire severity was not included as a separate explanatory variable and was therefore not explicitly tested. This operational design, however, reflects the actual conditions under which post-fire rehabilitation is implemented by forest-management authorities.

2.3. Vegetation and Soil Sampling and Analysis

Vascular plant composition was assessed during both monitoring years (2022 and 2023) between May and July using two 1 m × 1 m sub-quadrats within each experimental plot (Figure 3). One quadrat was placed in the central part of the eroded zone and the other in the middle of the depositional zone. Applying the same sampling window in both years ensured seasonal consistency across plots and rehabilitation structure types and allowed comparable recording of plant taxa, together with destructive harvesting of aboveground biomass. However, the May–July survey window may have underrepresented early spring annuals, ephemeral therophytes, and other short-lived Mediterranean taxa that complete most of their aboveground development before late spring or early summer [28]. Accordingly, the richness, density, cover, and composition values reported here should be interpreted as standardized May–July microsite-scale indicators rather than exhaustive full-season estimates of annual floristic richness. Because the same phenological window was applied in both years and across all microsites and structure types, comparisons among years, zones, and rehabilitation structures remain standardized.

The use of 1 m × 1 m quadrats was appropriate for the ecological scale and response variables examined in this study. The objective was to capture early post-fire vascular plant responses at the microsite level in direct association with rehabilitation structures rather than to provide a stand-level inventory of the burned forest. The recorded assemblages included both herbaceous and woody taxa. Since the study employed the same quadrat size and seasonal sampling period throughout, the design offered a consistent foundation for comparing recovery patterns across different structure types and microsites. However, the 1 m × 1 m quadrat design inevitably provides a conservative estimate of total plot-level floristic richness and may underrepresent sparsely distributed taxa. In particular, scattered woody species and patchily distributed shrubs may only be partially captured within a single quadrat, and their canopy cover may be underestimated when individuals extend beyond the quadrat boundaries. Therefore, richness and cover values are interpreted as microsite-scale indicators of vegetation response, not as exhaustive stand-level estimates.

https://doi.org/10.3390/ecologies7020059

Figure 3. Monitoring post-fire vegetation recovery using a 1 × 1 m sampling quadrat in a rehabilitated burned area. Visible rock fragments within the photographed quadrat represent natural coarse surface fragments derived from the local Tertiary parent material; their cover in this illustrative quadrat was visually estimated at approximately 15–40% of the surface.

The visible rock debris in Figure 3 was classified as natural coarse surface fragments derived from the local Tertiary parent material, rather than as soil contamination. Based on visual inspection of the photographed 1 × 1 m quadrat, the fragments were mainly gravel- to stone-sized rock fragments, and their visible surface cover was estimated as approximately 15–40% of the quadrat area, corresponding to a "many" coarse-fragment cover class. This estimate is provided only to describe the illustrative quadrat shown in Figure 3. Coarse-fragment cover was not measured systematically across all plots and was not included as a quantitative response variable. Before collecting mineral soil samples, loose surface litter, ash, roots, stones, and coarse organic debris were removed; therefore, the laboratory soil analyses refer to the upper 0–20 cm mineral soil fine-earth fraction.

Within each 1 m × 1 m quadrat, vascular plant cover was visually estimated as direct percentage cover, i.e., the percentage of ground area occupied by living vascular vegetation. The same field-estimation approach was applied consistently across all plots, microsites, structure types, and monitoring years in order to maintain comparability among sampling units. Cover estimation was based on the vertical projection of living aboveground vegetation within the quadrat boundaries. Field estimates were made by the same researcher throughout the study to minimize observer-related variability. Plant density was recorded as the number of field-identifiable vascular plant units per square meter. For solitary plants, each individual rooted within the quadrat was counted as one unit. For clonal or resprouting species with multiple shoots, such as *Pteridium aquilinum* and *Rubus canescens*, clearly separated ramets or shoots emerging from the soil surface within the quadrat were counted as field-countable units, because genet-level identification was not possible under field conditions. Species richness was calculated as the number of vascular plant taxa recorded in each quadrat. For floristic summaries, species and family composition were expressed as relative frequency (%) based on pooled presence records across the 36 microsite sampling units (9 plots × 2 microsites × 2 years). Each taxon was counted once per quadrat when recorded as present. Relative frequency was calculated as the number of quadrat records for a given taxon divided by the sum of quadrat records across all taxa in the pooled dataset, multiplied by 100. These values therefore represent normalized occurrence frequency and should not be interpreted as species abundance, cover, or biomass. For family-level summaries, all quadrat presence records of species belonging to the same family were pooled before calculating relative family frequency (%).

Aboveground biomass was determined by clipping all living aboveground plant material rooted within the quadrat at ground level, excluding belowground organs, coarse litter, and dead material. Samples were oven-dried (BINDER FED 400, BINDER GmbH, Tuttlingen, Germany) at 65 °C for 48 h and weighed to obtain dry aboveground biomass, expressed as grams per square metre (g m^{-2}). Plant identification was carried out using Flora Europaea [29–33], Euro + Med [34], Flora Hellenica [35,36], and Vascular Plants of Greece: An Annotated Checklist [37]. The classifications of life-form, chorological and status were based on research by Dimopoulos et al. [37] and Raunkiaer [38]. These attributes helped characterize floristic composition and aided in ecological interpretation of post-fire recovery across rehabilitation structures, especially regarding the contribution of woody versus herbaceous taxa and the balance between resprouting and seeding strategies.

Soil samples were collected from the upper 0–20 cm mineral soil layer in each plot × microsite combination. Samples were taken separately from eroded microsites, where soil material removal was evident, and from depositional microsites, where transported material had accumulated. Before sampling, loose surface litter, stones, roots, ash, and coarse organic debris were removed to standardize the sampled material across plots and microsites. Therefore, the reported soil properties refer to the upper mineral soil and should not be interpreted as measurements of the organic or humus horizon.

All soil samples were placed in labeled bags and transported to the laboratory. They were air-dried at 25 °C, gently passed through a 2-mm sieve, homogenized, and stored under controlled conditions until further analysis. Subsamples of the <2 mm fine-earth fraction were ground to powder using a ball mill for the determination of organic carbon, calcium carbonate, and total Kjeldahl nitrogen [39–41]. Soil structure was not classified as a pedological field descriptor because the analyses were based on disturbed, sieved mineral soil samples rather than undisturbed field observations. Therefore, the dataset allows the soil texture to be described as sandy loam but does not support a formal classification of natural aggregate structure, such as granular, blocky, platy, or massive.

Particle-size distribution was determined by the hydrometer method and expressed as sand, silt, and clay percentages (%). Calcium carbonate ($CaCO_3$) content was measured with a calcimeter after reaction with hydrochloric acid and expressed as $CaCO_3$ (%). Soil pH was measured electrometrically with a glass electrode in a soil:water suspension at a 1:2.5 ratio by weight and is reported as pH units. Electrical conductivity (EC) was measured with a conductivity meter in a 1:5 soil:water extract after shaking for 1 h and expressed as μS cm^{-1}. Organic carbon was determined after oxidation with sulfuric acid and potassium dichromate and expressed as organic C (%). Total nitrogen (total N) was determined as Kjeldahl nitrogen after sulfuric acid digestion and expressed as mg g^{-1}. Mineral nitrogen forms, ammonium nitrogen (NH_4-N) and nitrate nitrogen (NO_3-N), were determined in soil extracts and expressed as mg kg^{-1}. Exchangeable calcium (Ca), magnesium (Mg), potassium (K), and sodium (Na)were determined in soil extracts and expressed as meq 100 g^{-1} soil. Soil moisture was determined volumetrically and expressed as percentage water content (%). Soil moisture was measured only at the time of the annual soil-sampling campaigns and was included as a measured soil variable in the multivariate soil dataset. It was not monitored continuously throughout the experiment. No permanent soil-moisture sensors, repeated within-season measurements, or event-based measurements after rainfall were used. Therefore, the soil-moisture values represent the moisture status of the upper mineral soil at the sampling dates and should not be interpreted as continuous seasonal soil-water dynamics [39–41].

All analytical results were expressed on an air-dry soil basis before statistical analysis. To reduce analytical bias, all samples were treated under the same sampling depth, preparation, sieving, extraction and laboratory protocols. The instruments were calibrated before use using standard protocols and consistency was maintained by repeat testing and internal reference materials as appropriate.

2.4. Statistical Analyses

Statistical analyses were conducted on 18 plot × microsite sampling units, corresponding to nine plots × two microsite zones. These units were surveyed in two consecutive years, namely 2022 and 2023. Because the design included repeated observations within the same plots across years and microsites, vegetation responses were analyzed using generalized estimating equations (GEE). These equations provide population-averaged estimates for correlated longitudinal data without requiring specification of the full joint distribution of repeated measurements [42].

The analytical dataset comprised 36 repeated observations, corresponding to nine plots × two microsite zones × two monitoring years. Change-score analyses were based on 18 plot × microsite units, with each value representing the difference between 2023 and 2022.

To improve variance consistency, vegetation cover proportions were transformed using the arcsine square-root transformation before analysis. Vegetation density and aboveground biomass were log-transformed before analysis. For each vegetation response, the full model included year (2022, 2023), microsite zone (deposition vs. eroded), structure type (log barriers, wattles, and log dams), all interaction terms, and slope as a covariate. Significance of model terms was evaluated using Wald chi-square tests.

To evaluate the temporal recovery, change scores for each plot and zone were determined by subtracting the 2022 values from the 2023 values (Δ = value_{2023} − value_{2022}). Separate GEE models were then developed to analyze changes in vegetation cover, vegetation density, aboveground biomass, and selected soil variables (pH, total N, NH_4-N, NO_3-N, and electrical conductivity). These models used zone, structure type, zone × structure type, and slope as predictors, with plot treated as the clustering factor.

To provide a statistical comparison of floristic composition among rehabilitation structure types, a contingency-based analysis was applied to the species-level floristic occurrence dataset. Pooled presence records were cross-tabulated by vascular plant species and rehabilitation structure type, namely log barriers, wattles, and log dams, using the same occurrence data summarized in Supplementary Table S5. Rare species with fewer than five total occurrence records across all structure types were grouped as “Other” before analysis in order to reduce excessive sparsity in the contingency table. Pearson’s χ^2 test of independence was used to evaluate whether species-level floristic composition differed among structure types. Because several expected cell frequencies remained low, the asymptotic χ^2 result was supplemented with a Monte Carlo *p*-value based on fixed-margin random tables. Cramér’s V was calculated as an effect-size measure. This analysis was used as a categorical comparison of pooled species occurrence composition and was not interpreted as an abundance-, cover-, or biomass-based test.

To explore temporal changes in soil, the standardized soil variables were subjected to principal component analysis (PCA). Variables assessed were sand, clay, silt, pH, $CaCO_3$, organic carbon, total nitrogen, C/N, NH_4-N, NO_3-N, electrical conductivity (EC), exchangeable Ca, Mg, K, Na, available phosphorus (AP) and soil moisture. PCA was employed to summarize the complex interrelationships among soil parameters and to highlight variables that played important roles in the multivariate patterns [43]. Differences in multivariate soil composition across years, microsites, and structure types were examined using permutational multivariate analysis of variance (PERMANOVA), based on Euclidean distances and 4999 permutations [44]. Generalized estimating equation (GEE) models were fitted to the transformed vegetation response variables using a Gaussian family with an identity link and an exchangeable working correlation structure. Wald χ^2 tests were performed using robust sandwich standard errors. Because the study included only nine plot-level clusters, the GEE results were interpreted with caution. GEE was retained as an appropriate population-averaged framework for repeated observations within plots, because it accounts for within-cluster correlation without requiring full specification of the joint distribution of repeated measurements [42,45]. Nevertheless, small-sample GEE studies have shown that the conventional robust sandwich variance estimator can underestimate variance and produce liberal Wald-type tests when the number of independent clusters is small [46–48]. Accordingly, the GEE models were used primarily to summarize structure-, microsite-, and year-associated patterns while accounting for repeated plot-level observations. Statistical significance was interpreted alongside effect direction, effect magnitude, paired change-score results, and graphical consistency, rather than as stand-alone confirmatory evidence. Because very large Wald χ^2 statistics may occur when standard errors are small, particularly in small-cluster GEE applications and in models fitted to transformed proportional response variables, statistical inference was not based on Wald tests alone. For each vegetation response variable, model-based marginal estimates and 95% confidence intervals were additionally calculated for the main levels of year, microsite zone, and rehabilitation structure type. Model adequacy was evaluated by inspecting Pearson residuals plotted against fitted values and normal quantile–quantile plots of standardized residuals, which are provided in the Supplementary Materials. These diagnostic checks were used to assess whether residual patterns indicated strong deviations from model assumptions or influential lack of fit.

Principal component analysis (PCA) was conducted on standardized soil variables to summarize multivariate soil variation and identify the main variables contributing to the ordination patterns. All analyses were performed in Python 3.13 (Python Software Foundation, Wilmington, DE, USA) using pandas, numpy, statsmodels, scikit-learn, scipy, and scikit-bio.

3. Results

3.1. Vascular Plant Composition and Species Richness

The floristic dataset compiled from the vegetation records of PTH01–PTH09 included 36 microsite sampling units (9 plots × 2 microsites × 2 years) and comprised 27 vascular plant species belonging to 16 families. Species were ranked by relative frequency (%), calculated from pooled presence records across all microsite sampling units (Figure 4). *Cistus creticus* had the highest relative frequency (19.6%), followed by *Arbutus unedo* (12.8%) and *Smilax aspera* (8.4%). *Rosa canina* accounted for 6.7%, *Calicotome villosa* for 6.1%, *Dorycnium hirsutum* and *Rubus canescens* for 5.6% each, and *Pteridium aquilinum*, *Anthemis chia*, and *Trifolium campestre* for 4.5% each. These values represent normalized occurrence frequency across sampling units rather than abundance. Overall, the assemblage was dominated by a relatively small set of recurrent shrubs, climbers, and herbaceous taxa typical of early Mediterranean post-fire recovery.

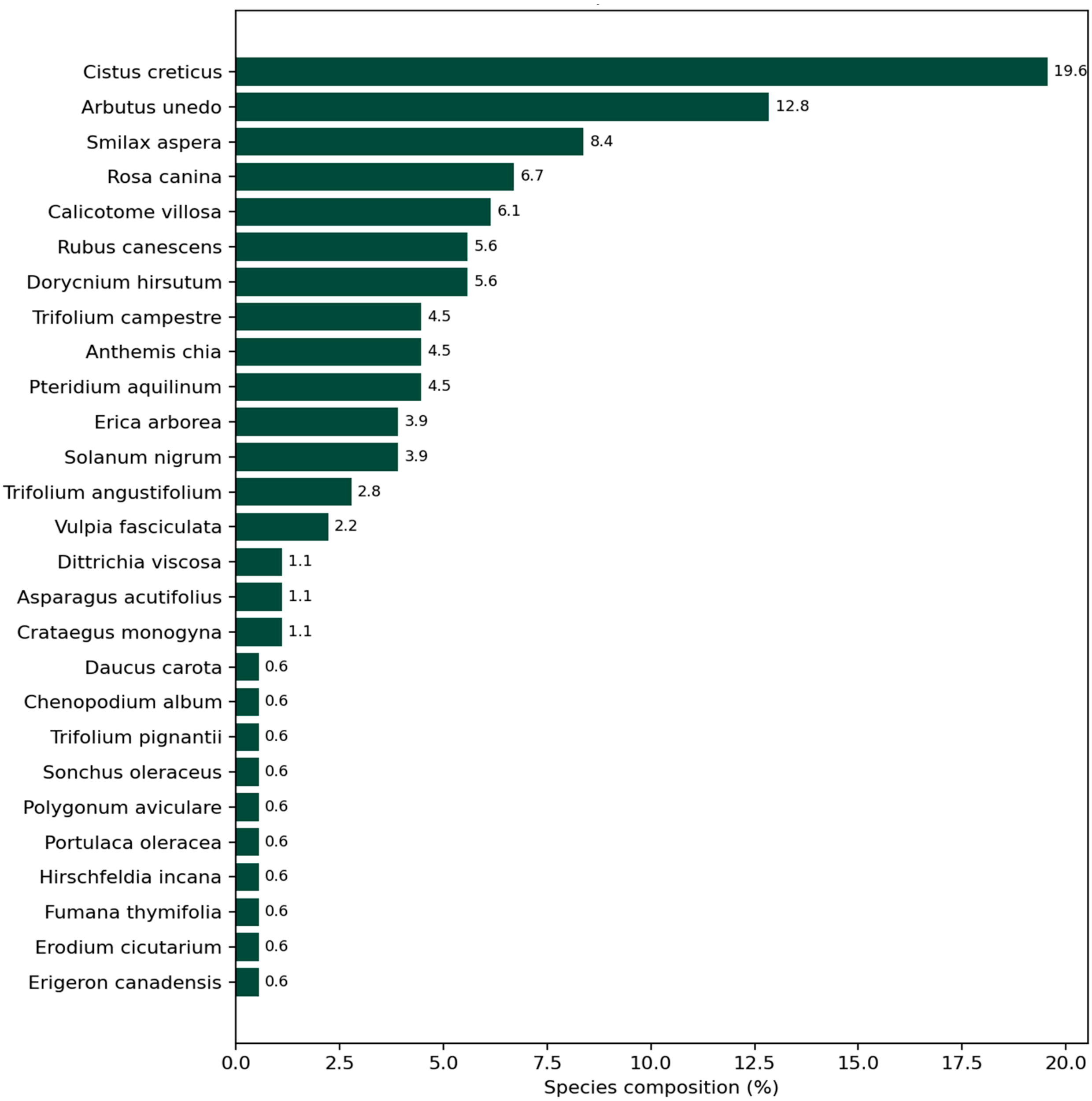

Figure 4. Relative frequency (%) of vascular plant species in Ancient Olympia based on pooled presence records across PTH01–PTH09.

At the family level, relative family frequency (%) was calculated by pooling the quadrat presence records of all species belonging to the same family across the 36 microsite sampling units. On this basis, Cistaceae had the highest relative family frequency (20.1%), followed by Fabaceae (19.6%) and Ericaceae (16.8%) (Figure 5). Rosaceae also accounted for a substantial proportion of pooled family records (13.4%), while Smilacaceae represented 8.4% and Asteraceae 6.7%. All remaining families each contributed less than 5% of the pooled family records. These values represent normalized occurrence frequency across sampling units rather than abundance. The post-fire vegetation of Ancient Olympia was therefore characterized mainly by taxa belonging to Cistaceae, Fabaceae, Ericaceae, and Rosaceae.

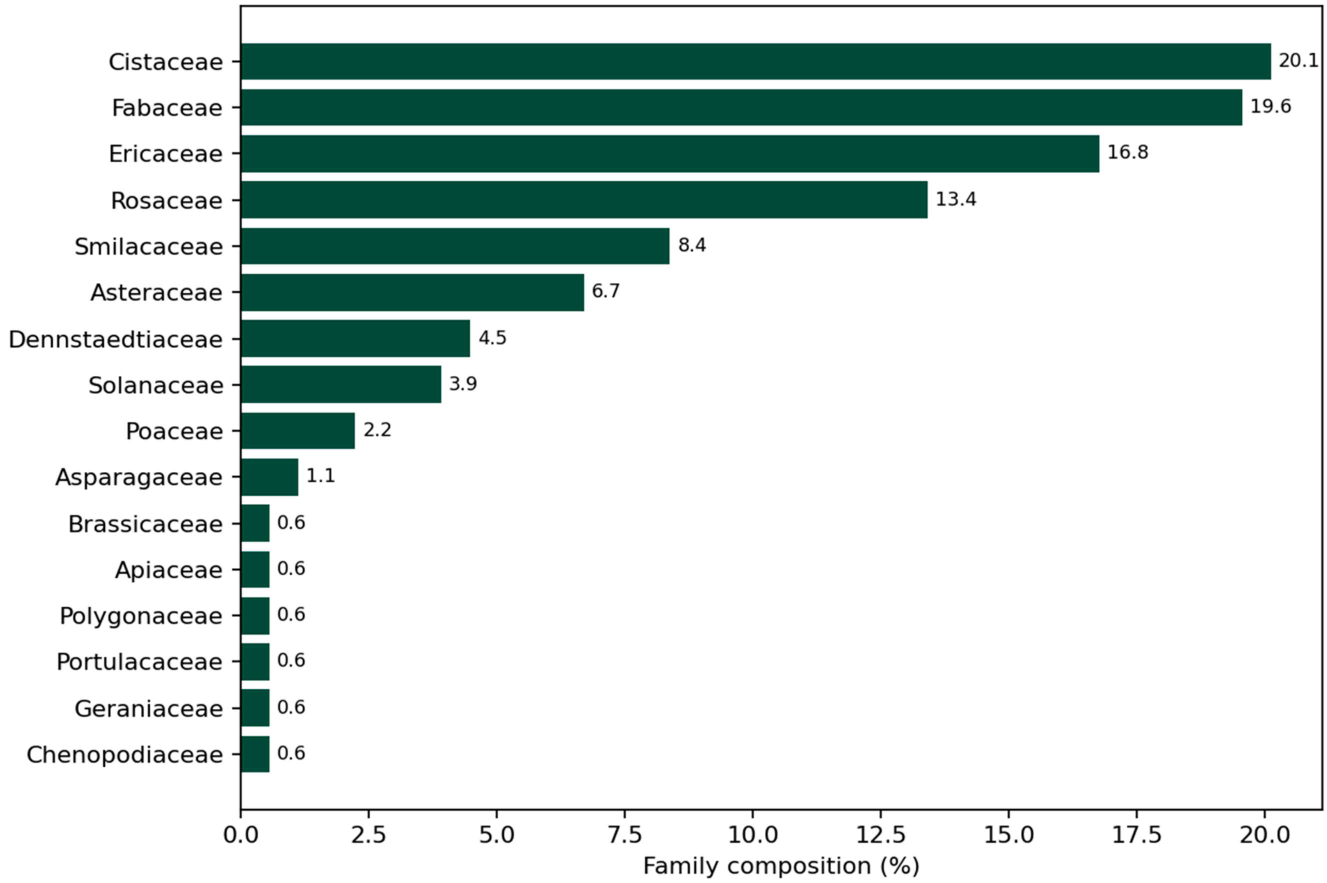

Figure 5. Relative frequency (%) of plant families in Ancient Olympia based on pooled presence records across PTH01–PTH09. Family-level values were obtained by pooling the quadrat presence records of all species belonging to each family.

Total species richness per microsite sampling unit increased from 2022 to 2023, and the increase was greater in depositional than in eroded microsites. Mean species richness increased from 4.11 species in depositional microsites and 3.78 species in eroded microsites in 2022 to 7.44 and 4.56 species, respectively, in 2023. Species-rich microsites were therefore more frequent in depositional zones. This pattern was consistent with the broader vegetation-recovery results and suggests that depositional microsites located immediately upslope of the rehabilitation structures provided more favorable conditions for species accumulation during early post-fire recovery.

Log dams had the highest cumulative species richness (21 recorded taxa), followed by log barriers (18 taxa) and wattles (13 taxa). At the family level, log dams contained 12 families, log barriers contained 11 families and wattles contained 9 families. In 2023, depositional microsites associated with log barriers and log dams supported an average of 8.0 species per sampling unit, while wattles supported 6.33 species per sampling unit. Differences in family-level composition were also seen across rehabilitation structure types (Figure 6). The greatest relative frequency in wattles was for Cistaceae (26.1%), followed by Ericaceae (23.9%), Fabaceae (19.6%) and Rosaceae (15.2%). In log barriers, the most abundant groups were Cistaceae and Fabaceae (20.0% each), followed by Ericaceae and Rosaceae (18.3% each). In log dams, Fabaceae was the most abundant family (19.2%), followed by Cistaceae (16.4%), Rosaceae (12.3%), Ericaceae (11.0%), Dennstaedtiaceae (9.6%), Smilacaceae (9.6%) and Solanaceae (8.2%).

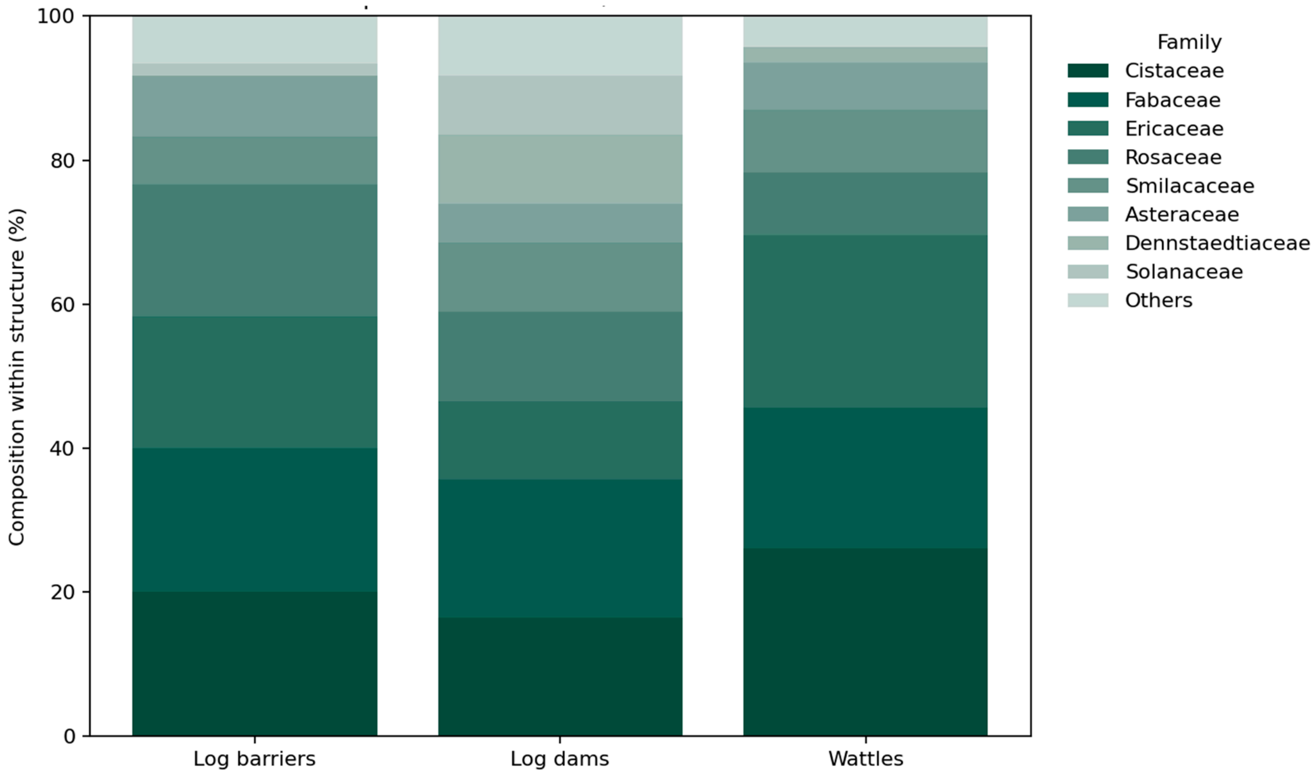

Figure 6. Relative family frequency (%) within each rehabilitation structure type in Ancient Olympia (log barriers, wattles, and log dams), based on pooled presence records across PTH01–PTH09.

The contingency-based comparison of species-level occurrence composition among structure types indicated marginal evidence of structure-associated floristic differentiation rather than a conventionally significant separation among structures (χ^2 = 37.68, degrees of freedom (df) = 26, asymptotic p = 0.0649; Monte Carlo p = 0.057; Cramér's V = 0.324). Inspection of the species occurrence profiles showed that log dams had a broader observed floristic spectrum, including higher occurrence of *Pteridium aquilinum*, *Solanum nigrum*, *Trifolium angustifolium*, *Rubus canescens*, and *Smilax aspera* relative to the other structure types. Overall, log dams showed the highest cumulative floristic richness and a broader observed floristic spectrum, but the statistical comparison provided only marginal support for structure-associated compositional differentiation.

3.2. Vegetation Responses Across Years, Microsites, and Structure Types

Vegetation responses showed a clear temporal recovery pattern between 2022 and 2023 (Table 5; Figure 7). Mean vegetation cover increased from 39.17 $\pm$ 21.44% in 2022 to 75.11 $\pm$ 12.90% in 2023. Because the Wald χ^2 statistic for the year effect was very large relative to the sample size, the result is reported together with model-based marginal estimates and 95% confidence intervals (CLs). The estimated marginal mean vegetation cover was 38.8% in 2022 (95% CI: 29.5–48.6) and 76.5% in 2023 (95% CI: 73.4–79.3), corresponding to an estimated increase of 37.5 percentage points (95% CI: 28.4–46.4). The temporal increase in vegetation cover was therefore interpreted primarily on the basis of the estimated effect size, its confidence interval, the paired change-score results, and diagnostic plots, rather than on the Wald χ^2 statistic alone. The increase in cover differed between microsites (year $\times$ zone: χ^2 = 4.88, p = 0.027) and among structure types (year $\times$ structure type: χ^2 = 7.09, p = 0.029), with greater increases in depositional microsites, particularly in plots associated with log barriers and log dams. Pearson residual and quantile-quantile (Q–Q) diagnostics indicated acceptable model fit, with residuals centered near zero and only mild deviations in the tails (Figures S1 and S2). Vegetation density increased from 22.56 ± 38.37 individuals per square metre (ind. m^{-2}) in 2022 to 39.89 ± 63.06 ind. m^{-2} in 2023 (year: $\chi^2 = 8.47$, $p = 0.004$). Plant density differed among structure types ($\chi^2 = 7.51$, $p = 0.023$) and showed a significant year × zone interaction ($\chi^2 = 8.29$, $p = 0.004$), indicating that temporal changes in plant density were microsite-dependent. Slope was also positively associated with vegetation density ($\chi^2 = 8.01$, $p = 0.005$). Back-transformed model-based marginal estimates showed an adjusted mean vegetation density of 9.9 ind. m^{-2} (95% CI: 7.7–12.4) in 2022 and 24.2 ind. m^{-2} (95% CI: 17.5–32.7) in 2023, corresponding to an estimated increase of 14.4 ind. m^{-2} (95% CI: 7.7–22.6).

Table 5. Summary of repeated-measures generalized estimating equation (GEE) GEE results for vegetation variables. Abbreviations: standard deviation (SD); confidence interval (CI); individuals per square metre (ind. m^{-2}).

Response Variable	2022 Mean ± SD	2023 Mean ± SD	Significant Model Terms
Vegetation cover (%)	39.17 ± 21.44	75.11 ± 12.90	Year: $\chi^2 = 1020.85$, $p < 0.001$; Year × Zone: $\chi^2 = 4.88$, $p = 0.027$; Year × Structure: $\chi^2 = 7.09$, $p = 0.029$, adjusted marginal means: 38.8% (95% CI: 29.5–48.6) in 2022 and 76.5% (95% CI: 73.4–79.3) in 2023, estimated increase: 37.5 percentage points (95% CI: 28.4–46.4)
Vegetation density, individuals per square metre (ind. m^{-2})	22.56 ± 38.37	39.89 ± 63.06	Year: $\chi^2 = 8.47$, $p = 0.004$; Structure: $\chi^2 = 7.51$, $p = 0.023$; Year × Zone: $\chi^2 = 8.29$, $p = 0.004$; Slope: $\chi^2 = 8.01$, $p = 0.005$, adjusted marginal means: 9.9 ind. m^{-2} (95% CI: 7.7–12.4) in 2022 and 24.2 ind. m^{-2} (95% CI: 17.5–32.7) in 2023; estimated increase: 14.4 ind. m^{-2} (95% CI: 7.7–22.6)
Aboveground biomass (g m^{-2})	203.83 ± 199.77	260.44 ± 227.30	Year: $\chi^2 = 12.96$, $p < 0.001$, adjusted marginal means: 113.2 g m^{-2} (95% CI: 77.4–159.0) in 2022 and 170.8 g m^{-2} (95% CI: 138.5–208.3) in 2023; estimated increase: 57.6 g m^{-2} (95% CI: 35.7–77.0)

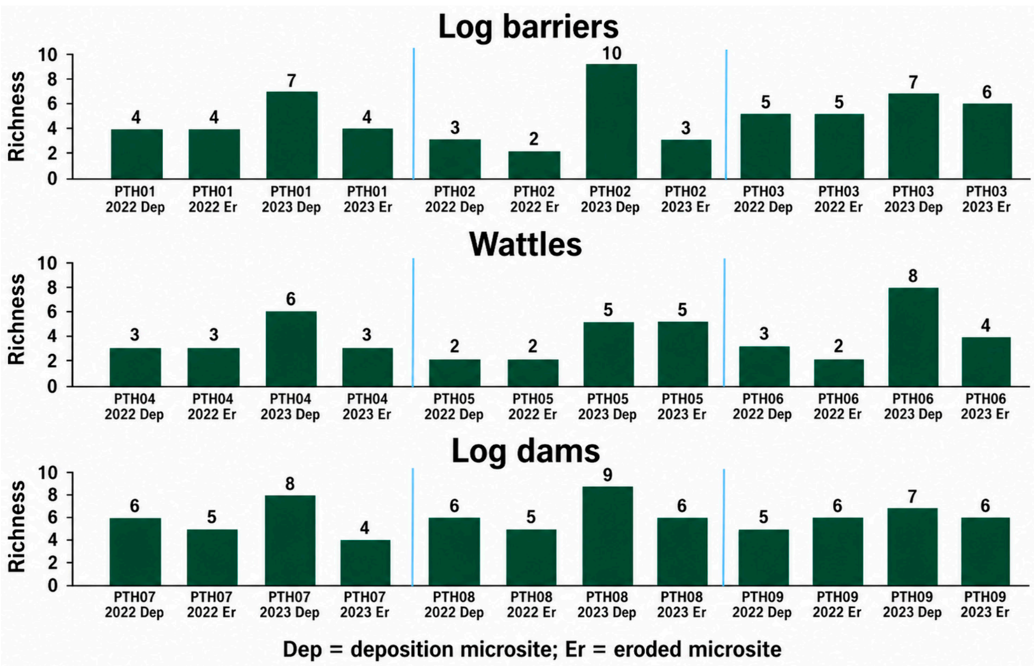

Figure 7. Species richness per microsite sampling unit in Ancient Olympia, shown separately for log barriers, wattles, and log dams. Deposition microsite (Dep); eroded microsite (Er).

Pearson residual and Q–Q diagnostics indicated acceptable model fit (Figures S3 and S4). The strongest increase in plant density was recorded in depositional microsites associated with wattles (Table 5; Figure 8).

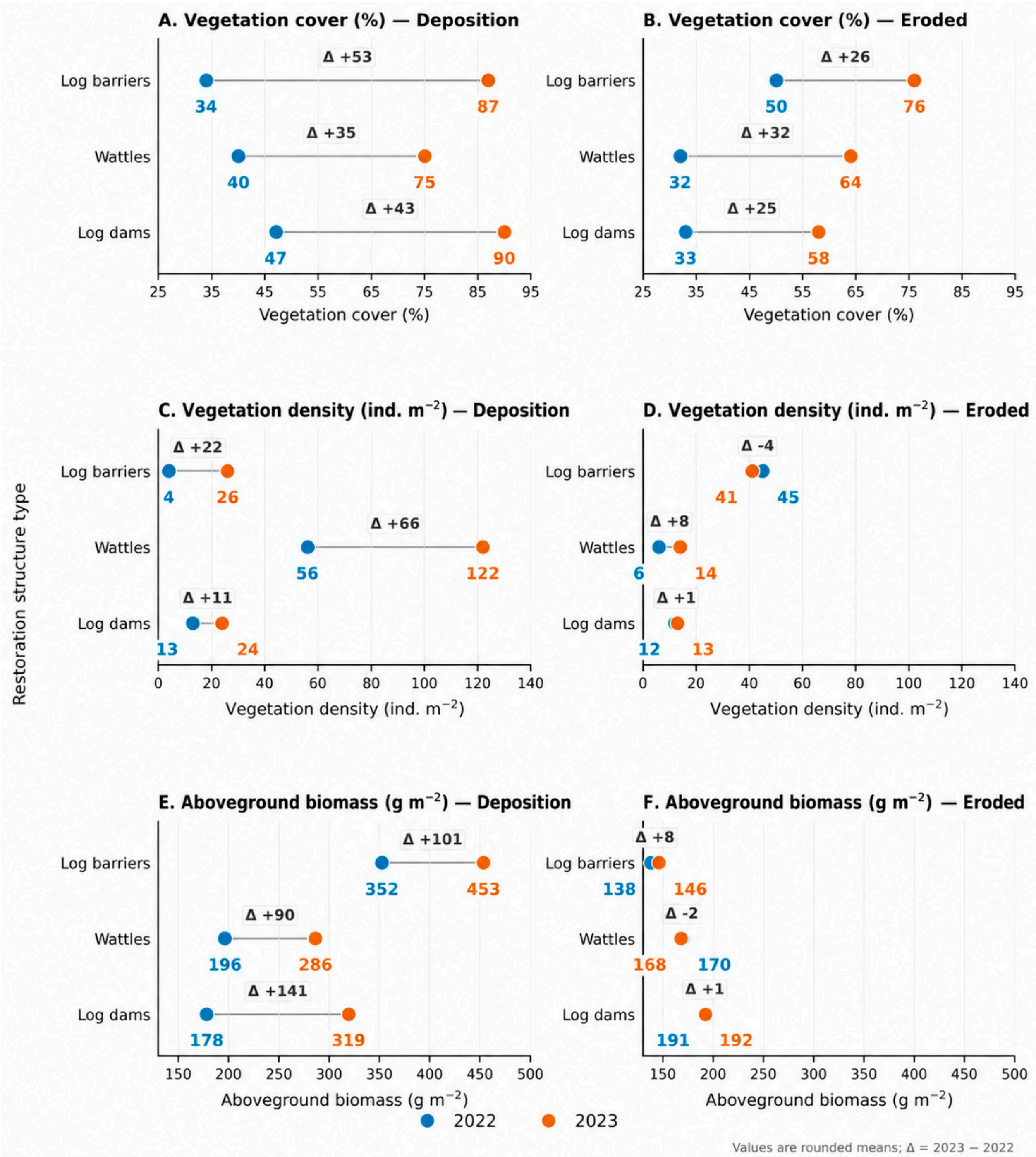

Figure 8. Microsite-dependent temporal recovery of vegetation cover, vegetation density, and aboveground biomass across post-fire rehabilitation structures from 2022 to 2023. Panels (**A**,**B**) show vegetation cover (%) in depositional and eroded microsites, respectively; panels (**C**,**D**) show vegetation density, individuals per square metre (ind. m^{-2}); and panels (**E**,**F**) show aboveground biomass (g m^{-2}). Points represent mean values for 2022 and 2023, grey lines connect paired annual means, and numbers above the lines indicate temporal change (Δ = 2023 − 2022). Values are rounded for visual clarity.

Aboveground dry biomass increased from 203.83 ± 199.77 g m^{-2} in 2022 to 260.44 ± 227.30 g m^{-2} in 2023. Year was a significant model term (χ^2 = 12.96, p < 0.001), whereas microsite zone and structure type were not significant interaction variables (Table 3; Figure 8). Back-transformed model-based marginal estimates showed an adjusted mean aboveground biomass of 113.2 g m^{-2} (95% CI: 77.4–159.0) in 2022 and 170.8 g m^{-2} (95% CI: 138.5–208.3) in 2023, corresponding to an estimated increase of 57.6 g m^{-2} (95% CI: 35.7–77.0). Pearson residual and Q–Q diagnostics indicated acceptable model fit (Figures S5 and S6). Overall, these results indicate strong early vegetation recovery across the monitored operational restoration area, with recovery patterns differing according to microsite condition and, for some variables, structure type.

3.3. Change-Score Analysis

The change-score analysis further showed that temporal recovery was stronger in deposition zones than in eroded zones (Table 6). Mean vegetation cover increased by 44.22 percentage points in deposition zones, compared with 27.67 percentage points in eroded zones. This difference was significant (zone: χ^2 = 4.53, p = 0.033), while cover change also differed among structure types (χ^2 = 14.57, p < 0.001).

Table 6. Summary of change-score analyses, expressed as delta (Δ = 2023 − 2022), for vegetation and selected soil variables. Mean Δ values are expressed in the units shown for each variable.

Variable	Mean Δ Deposition Zone	Mean Δ Eroded Zone	Significant Model Terms
Vegetation cover (%)	44.22	27.67	Zone: χ^2 = 4.53, p = 0.033; Structure: χ^2 = 14.57, p < 0.001
Vegetation density, individuals per square metre (ind. m^{-2})	33	1.67	Zone: χ^2 = 12.87, p < 0.001; Zone × Structure: χ^2 = 8.01, p = 0.018
Aboveground biomass (g m^{-2})	110.83	2.39	Zone: χ^2 = 14.99, p < 0.001; Structure: χ^2 = 37.62, p < 0.001; Slope: χ^2 = 65.90, p < 0.001
pH (pH units)	−0.76	−0.47	No significant effects
Total nitrogen N (total N) (mg g^{-1})	−1.18	−0.73	Zone × Structure: χ^2 = 10.23, p = 0.006
Ammonium nitrogen (NH_4-N) (mg kg^{-1})	−10.30	−6.68	Slope: χ^2 = 5.29, p = 0.021
Nitrate nitrogen (NO_3-N) (mg kg^{-1})	−57.97	−28.43	Structure: χ^2 = 13.57, p = 0.001; Zone × Structure: χ^2 = 12.98, p = 0.002; Slope: χ^2 = 16.19, p < 0.001
Electrical conductivity (µS cm^{-1})	−824.46	−289.64	Structure: χ^2 = 28.44, p < 0.001; Zone × Structure: χ^2 = 10.08, p = 0.006; Slope: χ^2 = 21.89, p < 0.001

Table note: Δ values represent the difference between 2023 and 2022 for each plot × microsite unit. Vegetation cover is expressed as percentage points; vegetation density as individuals per square metre (ind. m^{-2}); aboveground biomass as grams per square metre (g m^{-2}); pH as pH units; total nitrogen (total N) as mg g^{-1}; ammonium nitrogen (NH_4-N) and nitrate nitrogen (NO_3-N) as mg kg^{-1}; and electrical conductivity (EC) asmicrosiemens per centimetre (µS cm^{-1}).

Vegetation density increased by 33.00 ind. m^{-2} in deposition zones but by only 1.67 ind. m^{-2} in eroded zones, and this contrast was highly significant (zone: $\chi^2 = 12.87$, $p < 0.001$). In addition, the zone × structure type interaction was significant ($\chi^2 = 8.01$, $p = 0.018$), indicating that the magnitude of density change varied among structure–microsite combinations.

Biomass showed the clearest microsite contrast. Mean biomass increased by 110.83 g m^{-2} in deposition zones but by only 2.39 g m^{-2} in eroded zones (zone: $\chi^2 = 14.99$, $p < 0.001$). Biomass change also differed among structure types ($\chi^2 = 37.62$, $p < 0.001$), and slope was negatively associated with biomass change ($\chi^2 = 65.90$, $p < 0.001$). Across the monitored plots, the largest overall biomass increase was recorded in microsites associated with log dams. Selected soil variables showed pronounced declines between years. Mean pH declined by 0.61 units overall, but this change did not differ significantly among zones or structure types. Mean total N, NO_3-N, electrical conductivity, and NH4-N also declined, with significant patterning for several variables. The temporal change in total N varied according to the zone × structure type combination ($\chi^2 = 10.23$, $p = 0.006$). Similar structure–microsite-associated patterns were observed for NO_3-N ($\chi^2 = 12.98$, $p = 0.002$) and electrical conductivity ($\chi^2 = 10.08$, $p = 0.006$). In addition, NO_3-N and electrical conductivity were both significantly related to slope ($\chi^2 = 16.19$, $p < 0.001$ and $\chi^2 = 21.89$, $p < 0.001$, respectively).

All change-score values in Table 3 are expressed in the original measurement units of each response variable. Vegetation cover change is reported as percentage points, vegetation density as individuals per square metre (ind. m^{-2}), aboveground biomass as grams per square metre (g m^{-2}), pH as pH units, total nitrogen (total N) as mg g^{-1}, ammonium nitrogen (NH_4-N) and nitrate nitrogen (NO_3-N) as mg kg^{-1}, and electrical conductivity as microsiemens per centimetre (μS cm^{-1}).

3.4. Multivariate Soil Patterns

Principal component analysis (PCA) explained the dominant multivariate gradients in soil attributes during the initial post-fire monitoring period. The first two principal components explained 47.45% of the total variation, with the first principal component (PC1) explaining 33.43% and the second principal component (PC2) explaining 14.02% (Table 7, Figure 9). PC1 was mainly connected with NO_3-N, electrical conductivity, total N, exchangeable Ca, pH and organic C. PC2 was mainly associated with soil texture, specifically differences between sand, silt and clay. Overall, the samples from 2022 were characterized by larger PC1 values, while samples from 2023 changed to lower values of PC1. This pattern is consistent with the decrease in mineral N and conductivity-associated factors over time.

Although soil moisture was included in the multivariate soil dataset, it did not emerge among the main variables with the highest absolute PCA loadings. Accordingly, soil moisture was treated as a supporting soil variable rather than as a primary driver of the observed multivariate soil separation between 2022 and 2023. Because moisture was measured only at the annual sampling events, the results do not allow inference on continuous soil-moisture change throughout the experiment.

Table 7. Multivariate soil analysis. Abbreviations: principal component analysis (PCA); permutational multivariate analysis of variance (PERMANOVA); first principal component (PC1); second principal component (PC2); nitrate nitrogen (NO3-N); electrical conductivity (EC); total nitrogen (total N); exchangeable calcium (Ca); organic carbon (Org. C); calcium carbonate ($CaCO_3$).

A. PCA Summary		
Component	Variance explained (%)	Main contributing variables (highest absolute loadings)
PC1	33.43	NO_3-N (0.362), Electrical conductivity (0.361), Total N (0.336), Exchangeable Ca (0.334), pH (0.316), Org. C (0.302)
PC2	14.02	Sand (0.602), Silt (−0.514), Clay (−0.366), $CaCO_3$ (0.249)

B. PERMANOVA Results			
Factor	pseudo-F	R^2	*p*
Year	6.97	0.17	0.0002
Zone	2.76	0.075	0.011
Structure type	1.88	0.102	0.029

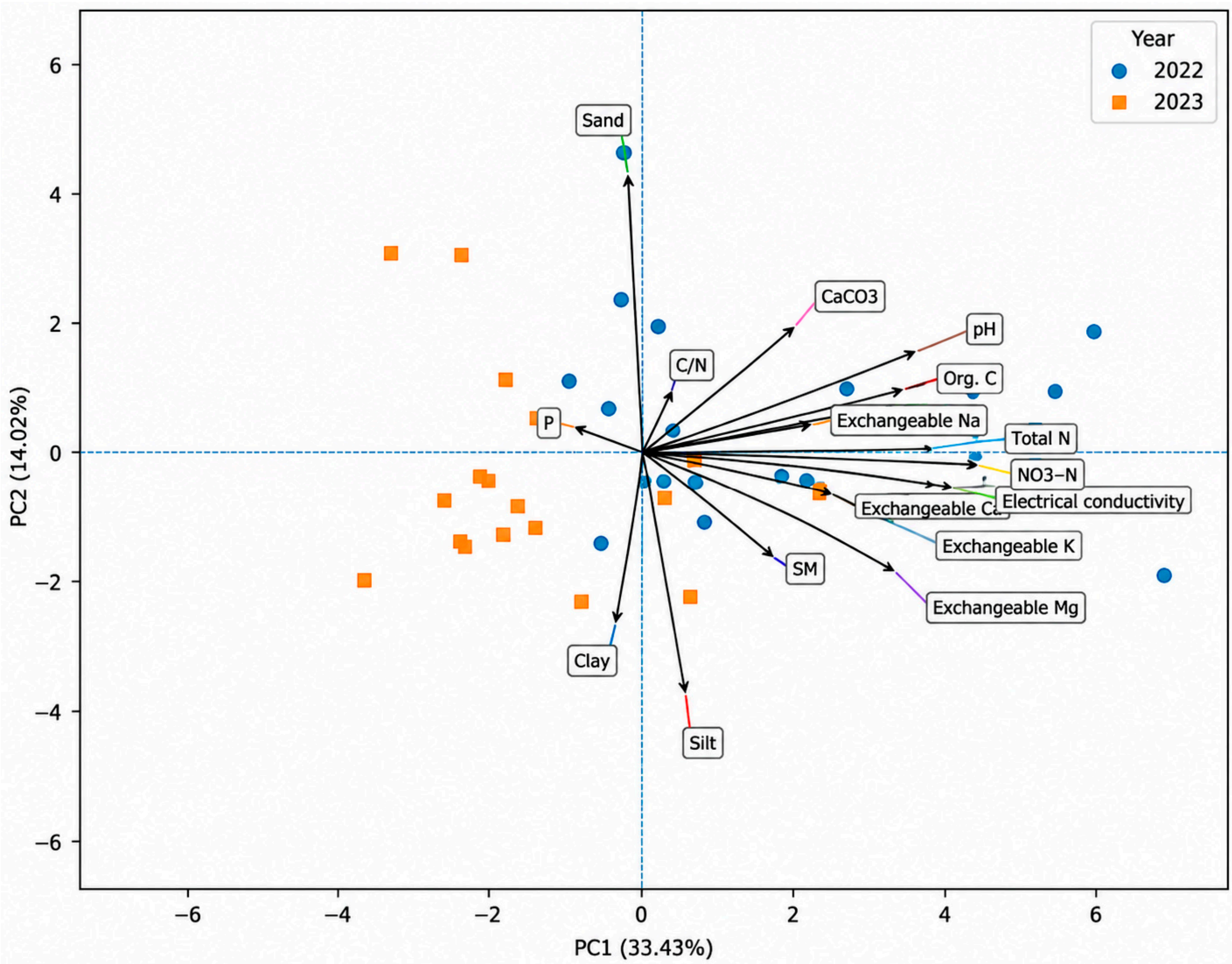

Figure 9. Principal component analysis (PCA) ordination of soil properties across sampling years. The first principal component (PC1) contributed 33.43% to the total variance and the second principal component (PC2) explained 14.02% of the variance. Samples from 2022 and 2023 largely separated along PC1, as characterized by mineral nitrogen, electrical conductivity, total nitrogen, pH and exchangeable calcium (Ca).

https://doi.org/10.3390/ecologies7020059

PERMANOVA indicated significant multivariate differences in soil properties between years (pseudo-F = 6.97, R^2 = 0.170, p = 0.0002), between microsites (pseudo-F = 2.76, R^2 = 0.075, p = 0.011) and among structure types (pseudo-F = 1.88, R^2 = 0.102, p = 0.029). As an indicator, soil pH changed from 7.31 ± 0.44 in 2022 to 6.69 ± 0.33 in 2023, total N from 2.00 ± 0.72 to 1.04 ± 0.28, NO_3-N from 54.16 ± 39.59 to 10.96 ± 8.18, EC from 1002.70 ± 622.82 to 445.65 ± 125.02, and NH_4-N from 13.17 ± 7.17 to 4.68 ± 3.20 (mean ± SD), supporting the PCA patterns and indicating a broad shift in soil chemical properties during early post-fire recovery.

4. Discussion

The burnt landscape of Ancient Olympia provided a clear indication of rapid early post-fire recovery between 2022 and 2023, with increases in vegetation cover, plant density, aboveground biomass and species richness. This pattern is consistent with the strong recovery capacity of many fire-prone Mediterranean ecosystems, where early re-establishment of vegetation is frequently achieved through resprouting, recruitment from persistent seed banks, and colonization by fast-growing herbaceous species [15,18]. The temporal recovery signal was spatially heterogeneous: depositional microsites consistently supported richer plant communities and greater increases in cover, density, and biomass than eroded microsites.

These structure–microsite-associated patterns can be interpreted through linked geomorphic, hydrological, and biological mechanisms. Wooden rehabilitation structures increase surface roughness and create low-energy depositional patches where runoff velocity is reduced and transported sediment, ash, litter fragments, organic matter, and plant propagules can accumulate. Such microsites may retain more near-surface moisture and provide a more protected substrate for seed retention, germination, resprouting, and early root establishment. This mechanism is consistent with previous post-fire studies showing that erosion-control barriers and related rehabilitation treatments can reduce sediment movement and modify runoff pathways, although their effectiveness depends on rainfall intensity, slope, soil properties, installation quality, and storage capacity [5,8,11–13,16]. It is also consistent with recent Greek evidence showing higher infiltration capacity in depositional zones than in adjacent eroded zones within post-fire rehabilitation structures [10]. Therefore, the stronger vegetation cover, density, biomass, and richness recorded in depositional microsites in the present study likely reflect the combined influence of sediment retention, moisture conservation, propagule trapping, and reduced physical disturbance. Because the present design was observational, these processes should be interpreted as plausible mechanistic pathways explaining the observed associations, rather than as experimentally demonstrated causal effects. The importance of this finding lies in the coupling between physical stabilization and biological recovery during the early post-fire window. In Mediterranean burned landscapes, the period before vegetation cover is re-established is often the phase of highest hydrological and geomorphological sensitivity, because bare soil surfaces are more exposed to runoff concentration, sediment detachment, and nutrient redistribution. The concentration of species richness, cover, density, and biomass in depositional microsites therefore suggests that rehabilitation structures may accelerate the transition from physically unstable burned surfaces to biologically stabilized recovery patches. This interpretation is consistent with evidence that post-wildfire erosion risk in Mediterranean landscapes is strongly influenced by the timing and spatial pattern of vegetation recovery, which modifies hydrological response and soil erodibility over time [5,16].

The floristic composition also supports the interpretation of an early Mediterranean post-fire recovery assemblage. Cistus creticus was the most frequent species, and Cistaceae, Fabaceae, and Ericaceae were well represented. These families include taxa with regeneration strategies characteristic of Mediterranean fire-prone vegetation, including post-fire seeding, resprouting, or mixed strategies [15,18]. Therefore, the observed community is best interpreted as a functionally filtered early recovery assemblage shaped by fire history, drought tolerance, and microsite resource retention, rather than as a full reconstruction of the pre-fire vegetation.

At the same time, the results do not support a simple interpretation that one rehabilitation structure type is universally superior. Log dams showed the highest cumulative floristic richness, wattles exhibited a marked increase in vegetation density, and log barriers also supported strong richness gains in depositional microsites during 2023. This suggests that structure performance is context-dependent and expressed through microsite formation rather than through a single, uniform treatment effect.

However, this context-dependent interpretation should be considered exploratory because the study included only three plots per rehabilitation structure type. This limited replication prevents robust conclusions regarding higher-order structure × microsite × year interactions and is particularly relevant for wattles, where the observed increase in plant density in depositional microsites was pronounced but based on a small number of plot-level replicates. Therefore, the structure-specific patterns reported here should be interpreted as operational field associations and hypothesis-generating evidence, rather than as definitive evidence of differential treatment performance among rehabilitation structures.

Comparable Mediterranean studies have likewise shown that post-fire management effects on vegetation may differ depending on the response variable considered, the local vegetation type, and the time elapsed since fire. Vegetation cover, woody recovery, and species diversity do not necessarily respond in the same direction or with the same intensity under different post-fire management strategies [49,50].

Recent Greek evidence strengthens this interpretation. A two-year study across Greek post-fire rehabilitation structures found that year was the dominant driver of vascular plant recovery, while structure-related ecological differences were still detectable in biodiversity patterns and indicator species responses. The Ancient Olympia results are in line with that broader pattern, but they add an important climatic contrast because this site belongs to the humid class of the UNEP aridity framework, unlike the semi-arid Greek burned landscapes examined elsewhere. The combination of stronger water availability at the regional scale and enhanced local resource accumulation in depositional microsites may therefore explain why vegetation recovery in Ancient Olympia was both rapid and spatially differentiated [21,23,24].

Soil pH decreased moderately from 7.31 ± 0.44 in 2022 to 6.69 ± 0.33 in 2023, but the soil reaction remained within the near-neutral to slightly alkaline range. This pattern is consistent with the predominantly calcareous substrate of the study area. All plots were developed on Tertiary deposits and contained carbonate material in the soil analytical dataset. Therefore, the observed pH change should not be interpreted as strong soil acidification. In calcareous soils, carbonate minerals can buffer pH changes by dissolving under acidic conditions, thereby limiting rapid acidification and reducing the magnitude of post-fire pH shifts [51].

A plausible explanation is that fire ash initially introduced alkaline compounds and base cations into the upper soil layer, temporarily increasing pH, electrical conductivity, and exchangeable cation availability [52,53]. During the following year, rainfall, runoff, erosion, leaching, plant uptake, and microbial immobilization may have redistributed or removed part of this transient post-fire input. This mechanism is consistent with the observed decreases in pH, EC, NH_4-N, NO_3-N, and total N between 2022 and 2023. In this context, the decrease in soil pH is better interpreted as the attenuation of a transient post-fire alkaline

https://doi.org/10.3390/ecologies7020059

pulse under carbonate-buffered conditions, rather than as unbuffered soil acidification. Because ash chemistry and carbonate dissolution rates were not measured directly, this interpretation should be regarded as a plausible explanation rather than as a directly tested mechanism. No data were collected about the post-fire ash chemistry or carbonate removal rates to determine the specific contribution of this mechanism or its true importance in the ecosystem dynamics, so it can only be presented here as a possible explanation.

At the microsite scale, depositional zones probably acted as resource-retention patches. Sediment and ash transported from upslope areas can accumulate behind wooden structures, together with organic residues and seeds. This can generate small-scale "fertility islands" where soil moisture, fine particles, organic material, and available nutrients are locally concentrated. Evidence from the related MoRe Forests soil study supports this interpretation: log-dam depositional zones showed higher conductivity, organic carbon, and Kjeldahl nitrogen than eroded zones, indicating enrichment of depositional microsites in soluble ions and organic-associated nitrogen [39]. In the present study, this mechanism is consistent with the stronger vegetation recovery observed in depositional microsites, particularly where structure-associated sediment and organic matter retention was more pronounced.

The visible coarse surface fragments observed in the field may also have influenced local erosion development and microsite differentiation. In the present study, these fragments are interpreted as natural rock fragments derived from the Tertiary parent material rather than as soil contamination. Under water-driven post-fire erosion, surface rock fragments can act as small-scale protective elements by reducing raindrop impact on the fine-earth fraction, limiting surface sealing, increasing surface roughness, slowing overland flow, and decreasing the transport capacity of runoff. In this way, they may contribute to lower sediment detachment and to localized sediment retention near rehabilitation structures. However, their effect is not necessarily uniform. Depending on fragment size, surface cover, spatial arrangement, degree of embedding, slope, and flow concentration, rock fragments may also divert runoff around individual fragments and generate small zones of local turbulence or preferential flow. Therefore, in the Ancient Olympia plots, rock debris should be interpreted as a potential microsite-scale modifier of water-driven erosion and deposition patterns. Because coarse-fragment cover was not systematically measured across all plots, its effect was not included as a quantitative explanatory variable and should be regarded as a plausible contributing factor rather than as a directly tested driver of erosion development [54–56].

The relationship between soil and vegetation recovery should also be understood as a feedback process. Improved microsite conditions may favour early plant establishment, while the developing vegetation can further stabilize the soil surface through canopy cover, litter input, root growth, and reduction in raindrop impact and runoff energy. These feedbacks are especially important in Mediterranean burned landscapes, where the interval between fire and vegetation re-establishment is often the period of greatest vulnerability to erosion and nutrient loss [5,16]. Thus, the parallel soil and vegetation changes observed in Ancient Olympia are best interpreted as coupled recovery processes: wooden structures were associated with microsite differentiation, depositional microsites retained more resources, and vegetation recovery progressively contributed to soil stabilization and nutrient cycling.

The stronger vegetation recovery in depositional microsites may also be linked to local hydrological improvement. A recent two-year Greek study on the same post-fire restoration framework showed that deposition zones consistently had greater infiltration capacity than adjacent erosion zones, and that these differences were particularly pronounced in Ancient Olympia. This hydrological contrast is highly relevant because short-term Mediterranean post-fire vegetation recovery is closely related to surface moisture availability and other near-surface environmental controls. In practical ecological terms, the depositional zones behind the structures may function as microsites of reduced stress, higher resource retention, and greater establishment probability, especially for early-successional taxa [10,17,19].

From a restoration perspective, these findings indicate that post-fire rehabilitation structures should not be evaluated only in engineering terms. Their ecological footprint is also important because they appear to influence where vegetation re-establishes more rapidly and where species richness accumulates most strongly during the first years after fire. In this sense, depositional microsites should not be regarded merely as sediment traps, but as biological hotspots of early recovery. This is particularly relevant in Mediterranean burned landscapes, where hydrological stabilization, vegetation recovery, and biodiversity reassembly are tightly linked processes rather than separate restoration targets [8,17].

At the level of plant functional ecology, the dominance of Cistus creticus and the strong representation of Cistaceae and Fabaceae are noteworthy because post-fire persistence in crown-fire ecosystems is largely organized by the combination of individual persistence through resprouting and population persistence through persistent seed banks. Functional-trait frameworks show that resprouting ability, seed-bank persistence, heat- or smoke-stimulated germination, and life-history strategy control early post-fire assembly and therefore determine whether microsites created by rehabilitation works become colonization sites or only temporary sediment-retention sites [57–60]. In this context, the Ancient Olympia assemblage should be interpreted not only as a list of recurrent taxa but also as a functionally filtered community shaped by fire, water availability, and microsite resource retention.

The results also contribute to the broader post-fire restoration literature for southern European forests, where management decisions often have to be made rapidly under uncertainty and with incomplete ecological information. Syntheses on post-fire management emphasize that emergency actions should be linked to longer-term ecosystem recovery objectives, including regeneration strategy, vegetation type, erosion risk, and future fire regime [61,62]. The Ancient Olympia case is particularly relevant in this respect because fire has long acted as an ecological and evolutionary force in Mediterranean landscapes, but contemporary restoration practice must now address the combined effects of severe wildfire, altered land use, climatic stress, and the need to protect both cultural landscapes and ecosystem functions [63].

The structure-specific patterns observed here should therefore be interpreted cautiously but practically. Studies on contour-felled logs, straw wattles, mulches, and forest-residue applications show that post-fire treatment effectiveness depends strongly on rainfall intensity, slope, sediment storage capacity, installation quality, ground cover, treatment decay, and the timing of the first erosive storms [64–66].

This general context is also consistent with the meteorological conditions recorded during the wildfire and post-fire monitoring period. As reported in Section 2.1, annual mean air temperature was very similar in 2021, 2022, and 2023, whereas annual precipitation showed stronger interannual variability. The wildfire year, 2021, was much wetter, with 1145 mm of precipitation, compared with 667 mm in 2022 and 771 mm in 2023. This contrast is relevant because the effectiveness of post-fire rehabilitation structures is strongly linked to rainfall-driven runoff generation, sediment detachment, and sediment storage behind the structures. The relatively wet wildfire year may have increased the potential for early post-fire runoff and sediment redistribution, while the lower precipitation totals during the two monitoring years may have allowed vegetation recovery and depositional microsite stabilization to proceed under less extreme annual rainfall conditions. However, because event-scale rainfall intensity and the exact timing of the first erosive storm were not monitored at the plot scale, these meteorological data are used here as annual hydroclimatic context rather than as direct evidence of storm-event effects [10].

These studies support the interpretation that log barriers, wattles, and log dams are unlikely to produce a single uniform ecological response. Their effects are likely to operate locally through hydrological and geomorphic modifications that create favourable microhabitats in some microsites but provide weaker ecological benefits in others.

The interaction between soil and vegetation presented here should be discussed combined with the changes in post-fire soil physical and chemical properties. Fire can influence soil water repellency, runoff paths, nutrient availability, pH and electrical conductivity. Ash inputs can transiently enhance pH and nutrient pools, but these benefits may subsequently decrease due to runoff, leaching, erosion, microbial immobilization and plant uptake [67–70]. Decreases in mineral nitrogen, pH and electrical conductivity from 2022 to 2023 are detected that are compatible with a brief post-fire nutrient pulse followed by redistribution and biological uptake. This points to the necessity of assessing vegetation and soils together since post-fire soil conditions affect vegetation recovery and vegetation, in turn, impacts subsequent soil stabilization and nutrient cycling.

From a management perspective, these findings suggest that post-fire rehabilitation structures should be planned and evaluated not only according to their capacity to reduce runoff and sediment export, but also according to their potential to support vegetation establishment, plant diversity, and early ecosystem recovery. In particular, depositional microsites formed upslope of log barriers, wattles, and log dams may function as early recovery nuclei where sediment, organic material, moisture, and propagules accumulate. Therefore, post-fire monitoring protocols in Mediterranean burned landscapes should integrate vegetation-based indicators, such as species richness, vegetation cover, plant density, and aboveground biomass, alongside conventional hydrological and erosion-control metrics. Such an integrated assessment would allow managers to identify which structure–microsite combinations most effectively support both physical stabilization and ecological recovery during the first post-fire years.

5. Limitations and Future Research Directions

Several limitations should be considered when interpreting the results of this study. First, the research was conducted within operationally installed post-fire rehabilitation works rather than within a fully randomized experimental framework. Consequently, the comparisons among structure types should be interpreted as structure- and microsite-associated patterns within a restored burned landscape, not as strict causal treatment effects against an untreated control. Second, fire severity was not explicitly incorporated as an explanatory variable, and no unburned or untreated burned control plots were included. These constraints limit the ability to separate the effects of rehabilitation structures from other spatially variable post-fire drivers.

Third, the number of plots per structure type was necessarily limited, with three plots assigned to each rehabilitation structure type. This constraint is common in operational field studies but limits statistical generalization, particularly for higher-order structure × microsite × year interactions. It is also relevant to the GEE analyses, because the nine plot-level clusters provide limited support for fully robust sandwich-based inference. Therefore, the reported Wald χ^2 tests should be interpreted as exploratory indicators of repeated-measures associations, and the conclusions rely primarily on the consistency of effect directions, observed changes, confidence intervals, and microsite-level recovery patterns.

Fourth, the vegetation sampling design was based on 1 × 1 m quadrats. This quadrat size was suitable for standardized microsite-scale comparisons close to post-fire rehabilitation structures, but it may provide conservative estimates of total plot-level floristic richness and vegetation cover. This limitation is particularly relevant for woody vegetation, scattered shrubs, patchily distributed resprouting species, and individuals whose canopy or clonal spread extended beyond the quadrat boundaries. Therefore, the richness, cover, density, and biomass values reported here should be interpreted as microsite-scale indicators of early vegetation response rather than as exhaustive stand-level estimates of the full woody and herbaceous community.

Fifth, the floristic surveys were performed during a single fixed May–July sampling window. This improved comparability among years, microsites, and rehabilitation structure types, but it may have led to underrepresentation of early spring annuals, ephemeral therophytes, and taxa with short aboveground life cycles that completed flowering or senescence before sampling. As a result, the reported species richness values should be interpreted as conservative estimates of the vegetation detectable during the survey period, not as complete annual floristic richness. This seasonal constraint may also have influenced the recorded community-composition patterns by favouring longer-persisting herbs, perennial species, resprouting shrubs, and late-season taxa.

Finally, no pre-fire characterization of the plant community was available for the monitored plots. Consequently, the study cannot quantify floristic change relative to a documented pre-fire baseline or determine how closely the observed post-fire assemblages approximate the pre-fire vegetation. The results therefore describe early post-fire vegetation recovery and structure-associated microsite patterns during 2022–2023, rather than direct departures from, or recovery toward, a measured pre-fire plant community. These limitations point to several future research priorities. Continued monitoring is needed to determine whether the initial benefits observed in depositional microsites persist during the first post-fire years and, more importantly, whether they lead to longer-term differences in species diversity, woody vegetation development, forest structure, and watershed hydrological function. Future studies should ideally include larger numbers of plots, broader spatial replication, untreated burned control sites, unburned reference sites, and, where available, pre-fire floristic data or contemporary unburned analogues to strengthen assessments of recovery.

Repeated seasonal surveys, including early spring and late-season sampling, would improve detection of ephemeral annuals and provide more complete estimates of annual floristic richness. Future work should also integrate explicit fire-severity metrics, direct measurements of sediment accumulation, soil moisture and hydrological response, and trait-based or demographic analyses, including regeneration strategy, life form, resprouting intensity, seedling recruitment, and seed-bank dynamics. Such integrated designs would help clarify the mechanisms through which rehabilitation structures and the microsites they create influence vegetation recovery in Mediterranean burned landscapes.

6. Conclusions

In this observational study conducted within operationally implemented post-fire rehabilitation works, vegetation cover, plant density, aboveground biomass, and species richness increased markedly between 2022 and 2023, indicating rapid early post-fire recovery during the first two years after wildfire. Recovery signals were consistently stronger in depositional microsites than in eroded microsites, suggesting that these microsites were associated with more favourable local conditions for plant establishment. This pattern is consistent with the expected accumulation of sediment, organic material, moisture, and propagules upslope of wooden rehabilitation structures, although the observational design does not allow strict causal attribution. The recovering vegetation was dominated by *Cistus creticus* and by plant families typical of Mediterranean post-fire communities, particularly Cistaceae, Fabaceae, and Ericaceae.

The three rehabilitation structure types were associated with distinct recovery patterns, but no single structure type was clearly superior across all response variables. Log barriers, wattles, and log dams were linked to different structure–microsite combinations. Significant changes in soil properties during the monitoring period further indicate that vegetation recovery coincided with a broader reorganization of the post-fire soil environment.

Overall, the results suggest that post-fire rehabilitation structures should be evaluated not only according to their capacity to reduce runoff and soil loss, but also according to their potential to enhance vegetation recovery, plant diversity, and ecosystem resilience. In the burned landscape of Ancient Olympia, depositional microsites associated with wooden rehabilitation structures appeared to function as early nuclei of ecological recovery, where vegetation structure, species richness, and soil processes began to reorganize together. This microsite-based perspective highlights the multifunctional role of post-fire rehabilitation structures in Mediterranean burned landscapes and provides a useful framework for integrating biodiversity recovery into future post-fire restoration planning. Mechanistically, the stronger recovery signals in depositional microsites are consistent with sediment, ash, organic matter, nutrient, moisture, and propagule retention behind wooden rehabilitation structures, followed by feedback between increasing vegetation cover and soil-surface stabilization.

These findings should be interpreted as structure- and microsite-associated recovery patterns under operational restoration conditions, rather than as definitive causal treatment effects.

For land managers, the main operational message is that post-fire rehabilitation structures should be planned, maintained, and monitored as multifunctional interventions rather than as erosion-control measures alone. In practical terms, monitoring should focus not only on whether structures reduce runoff and sediment export, but also on whether they generate stable depositional microsites that retain sediment, organic material, moisture, and propagules and thereby support early vegetation establishment. Vegetation cover, species richness, plant density, and aboveground biomass can therefore serve as rapid field indicators of ecological recovery alongside conventional erosion and hydrological indicators. Under Mediterranean post-fire conditions, managers should prioritize the maintenance of structures and microsites that show both physical stability and early vegetation response, while avoiding the assumption that a single structure type is universally superior across all sites.

Supplementary Materials: The following supporting information can be downloaded at: https://www.mdpi.com/article/10.3390/ecologies7020059/s1, Table S1: Vascular plant species and their families recorded in Ancient Olympia across PTH01–PTH09, organized by plot, structure type, year, and microsite sampling unit; Table S2: Vascular Plant Species composition (%) in Ancient Olympia based on pooled occurrence records across PTH01–PTH09; Table S3: Family composition (%) in Ancient Olympia based on pooled occurrence records across PTH01–PTH09; Table S4: Family richness and composition per structure type in Ancient Olympia across PTH01–PTH09; Table S5: Vascular plant species richness and composition per structure type in Ancient Olympia across PTH01–PTH09; Figures S1–S6: Pearson residual and Q–Q diagnostic plots for the vegetation-response models.

Author Contributions: Conceptualization, A.D.S.; methodology, A.D.S.; formal analysis, A.D.S.; investigation, A.D.S., N.P. and P.M.; resources, A.D.S., N.P., P.M., A.B. and P.L.; data curation, A.D.S. and P.M.; writing—original draft preparation, A.D.S.; writing—review and editing, A.D.S., N.P., P.M., A.B. and P.L.; visualization, A.D.S. and N.P.; supervision, A.D.S.; project administration, N.P.; funding acquisition, N.P. All authors have read and agreed to the published version of the manuscript.

Funding: This research was financially supported by the Hellenic Green Fund, grant number 21SYMV008996029 2021-07-28, with beneficiary the Directorate General for Forests and Forest Environment of the Hellenic Ministry of Environment and Energy. Research Project: MoRe Forests "MOnitoring the impact of REstoration works in the post-fire Forest environment in Greece".

Informed Consent Statement: Not applicable.

Data Availability Statement: The data supporting the findings of this study are provided in the Supplementary Materials. Additional information is available from the corresponding author upon reasonable request.

Acknowledgments: The authors acknowledge the personnel of the Directorate General for Forests and Forest Environment for administrative support, as well as the Forest Directorate of Ilia and the Pyrgos Forest Service for their support during the implementation of this research. We also thank everyone who contributed in any way to the implementation of this research.

Conflicts of Interest: The authors declare no conflicts of interest.

References

1. Cunningham, C.X.; Williamson, G.J.; Bowman, D.M.J.S. Increasing frequency and intensity of the most extreme wildfires on Earth. *Nat. Ecol. Evol.* **2024**, *8*, 1420–1425. [CrossRef] [PubMed]
2. Giannaros, T.M.; Papavasileiou, G. Changes in European fire weather extremes and related atmospheric drivers. *Agric. For. Meteorol.* **2023**, *342*, 109749. [CrossRef]
3. El Garroussi, S.; Di Giuseppe, F.; Barnard, C.; Wetterhall, F. Europe faces up to tenfold increase in extreme fires in a warming climate. *npj Clim. Atmos. Sci.* **2024**, *7*, 30. [CrossRef]
4. Keeley, J.E. Fire intensity, fire severity and burn severity: A brief review and suggested usage. *Int. J. Wildland Fire* **2009**, *18*, 116–126. [CrossRef]
5. Shakesby, R.A. Post-wildfire soil erosion in the Mediterranean: Review and future research directions. *Earth-Sci. Rev.* **2011**, *105*, 71–100. [CrossRef]
6. Certini, G. Effects of fire on properties of forest soils: A review. *Oecologia* **2005**, *143*, 1–10. [CrossRef] [PubMed]
7. Neary, D.G.; Klopatek, C.C.; DeBano, L.F.; Ffolliott, P.F. Fire effects on belowground sustainability: A review and synthesis. *For. Ecol. Manag.* **1999**, *122*, 51–71. [CrossRef]
8. Girona-García, A.; Vieira, D.C.S.; Silva, J.; Fernández, C.; Robichaud, P.R.; Keizer, J.J. Effectiveness of post-fire soil erosion mitigation treatments: A systematic review and meta-analysis. *Earth-Sci. Rev.* **2021**, *217*, 103611. [CrossRef]
9. Proutsos, N.; Solomou, A.; Michopoulos, P.; Bourletsikas, A.; Stefanidis, S. *Investigation of the Effectiveness of Flood and Erosion Control Works in Burned Areas*; Final Technical Report/Project Deliverable of the MoRe Forests Project; Institute of Mediterranean Forest Ecosystems, ELGO-DIMITRA: Athens, Greece, 2024.
10. Proutsos, N.D.; Stefanidis, S.P.; Solomou, A.D.; Michopoulos, P.; Bourletsikas, A.; Lattas, P. Impact of post-fire rehabilitation treatments on forest soil infiltration in Mediterranean landscapes: A two-year study. *Fire* **2025**, *8*, 269. [CrossRef]
11. Robichaud, P.R.; Wagenbrenner, J.W.; Brown, R.E.; Wohlgemuth, P.M.; Beyers, J.L. Evaluating the effectiveness of contour-felled log erosion barriers as a post-fire runoff and erosion mitigation treatment in the western United States. *Int. J. Wildland Fire* **2008**, *17*, 255–273. [CrossRef]
12. Wagenbrenner, J.W.; MacDonald, L.H.; Rough, D. Effectiveness of three post-fire rehabilitation treatments in the Colorado Front Range. *Hydrol. Process.* **2006**, *20*, 2989–3006. [CrossRef]
13. Robichaud, P.R.; Ashmun, L.E.; Sims, B.D. *Post-Fire Treatment Effectiveness for Hillslope Stabilization*; General Technical Report RMRS-GTR-240; U.S. Department of Agriculture, Forest Service, Rocky Mountain Research Station: Fort Collins, CO, USA, 2010; 62p.
14. Suding, K.N.; Gross, K.L.; Houseman, G.R. Alternative states and positive feedbacks in restoration ecology. *Trends Ecol. Evol.* **2004**, *19*, 46–53. [CrossRef] [PubMed]
15. Bond, W.J.; Keeley, J.E. Fire as a global herbivore: The ecology and evolution of flammable ecosystems. *Trends Ecol. Evol.* **2005**, *20*, 387–394. [CrossRef] [PubMed]
16. Cerdà, A.; Doerr, S.H. Influence of vegetation recovery on soil hydrology and erodibility following fire: An 11-year investigation. *Int. J. Wildland Fire* **2005**, *14*, 423–437. [CrossRef]
17. Menéndez-Miguélez, M.; Cañellas, I.; Erdozain, M.; de-Miguel, S.; Alberdi, I. Post-fire treatments in Mediterranean forests: A review for enhancing restoration strategies. *Fire Ecol.* **2025**, *21*, 82. [CrossRef]
18. Pausas, J.G.; Keeley, J.E. Evolutionary ecology of resprouting and seeding in fire-prone ecosystems. *New Phytol.* **2014**, *204*, 55–65. [CrossRef] [PubMed]
19. Fernández-Guisuraga, J.M.; Fernandes, P.M.; Tárrega, R.; Beltrán-Marcos, D.; Calvo, L. Vegetation recovery drivers at short-term after fire are plant community-dependent in Mediterranean burned landscapes. *For. Ecol. Manag.* **2023**, *539*, 121034. [CrossRef]

20. Kazanis, D.; Arianoutsou, M. Long-term post-fire vegetation dynamics in *Pinus halepensis* forests of Central Greece: A functional group approach. *Plant Ecol.* **2004**, *171*, 101–121. [CrossRef]
21. Solomou, A.D.; Proutsos, N.; Michopoulos, P.; Bourletsikas, A. Monitoring plant biodiversity and indicator species across post-fire rehabilitation structures in Greece: A two-year study. *Fire* **2026**, *9*, 152. [CrossRef]
22. Ministry of Climate Crisis and Civil Protection. 2021-EMSR528-Fire in Ancient Olympia. Available online: https://civilprotection.gov.gr/copernicus/2021-emsr528-pyrkagia-sti-arhaia-olympia (accessed on 14 April 2026).
23. Proutsos, N.D.; Tsiros, I.X.; Nastos, P.; Tsaousidis, A.A. A note on some uncertainties associated with Thornthwaite's aridity index introduced by using different potential evapotranspiration methods. *Atmos. Res.* **2021**, *260*, 105727. [CrossRef]
24. Tsiros, I.X.; Nastos, P.; Proutsos, N.D.; Tsaousidis, A. Variability of the aridity index and related drought parameters in Greece using climatological data over the last century (1900–1997). *Atmos. Res.* **2020**, *240*, 104914. [CrossRef]
25. UNEP. *World Atlas of Desertification*; Edward Arnold: London, UK, 1992.
26. Thornthwaite, C.W. An approach toward a rational classification of climate. *Geogr. Rev.* **1948**, *38*, 55–94. [CrossRef] [PubMed]
27. IUSS Working Group WRB. *World Reference Base for Soil Resources. International Soil Classification System for Naming Soils and Creating Legends for Soil Maps*, 4th ed.; International Union of Soil Sciences (IUSS): Vienna, Austria, 2022.
28. Pescador, D.S.; Sánchez, A.M.; Luzuriaga, A.L.; Sierra-Almeida, A.; Escudero, A. Winter is coming: Plant freezing resistance as a key functional trait for the assembly of annual Mediterranean communities. *Ann. Bot.* **2018**, *121*, 335–344. [CrossRef]
29. Tutin, T.G.; Heywood, V.H.; Burges, N.A.; Moore, D.M.; Valentine, D.H.; Walters, S.M.; Webb, D.A. (Eds.) *Flora Europaea, Volume 1: Lycopodiaceae to Platanaceae*; Cambridge University Press: Cambridge, UK, 1964.
30. Tutin, T.G.; Heywood, V.H.; Burges, N.A.; Moore, D.M.; Valentine, D.H.; Walters, S.M.; Webb, D.A. (Eds.) *Flora Europaea, Volume 2: Rosaceae to Umbelliferae*; Cambridge University Press: Cambridge, UK, 1968.
31. Tutin, T.G.; Heywood, V.H.; Burges, N.A.; Moore, D.M.; Valentine, D.H.; Walters, S.M.; Webb, D.A. (Eds.) *Flora Europaea, Volume 3: Diapensiaceae to Myoporaceae*; Cambridge University Press: Cambridge, UK, 1972.
32. Tutin, T.G.; Heywood, V.H.; Burges, N.A.; Moore, D.M.; Valentine, D.H.; Walters, S.M.; Webb, D.A. (Eds.) *Flora Europaea, Volume 4: Plantaginaceae to Compositae (and Rubiaceae)*; Cambridge University Press: Cambridge, UK, 1976.
33. Tutin, T.G.; Heywood, V.H.; Burges, N.A.; Moore, D.M.; Valentine, D.H.; Walters, S.M.; Webb, D.A. (Eds.) *Flora Europaea, Volume 5: Alismataceae to Orchidaceae (Monocotyledones)*; Cambridge University Press: Cambridge, UK, 1980.
34. Euro + Med. Euro + Med PlantBase—The Information Resource for Euro-Mediterranean Plant Diversity. Available online: https://europlusmed.org (accessed on 14 April 2026).
35. Strid, A.; Tan, K. (Eds.) *Flora Hellenica*; Koeltz Scientific Books: Königstein, Germany, 1997; Volume 1.
36. Strid, A.; Tan, K. (Eds.) *Flora Hellenica*; Koeltz Scientific Books: Königstein, Germany, 2002; Volume 2.
37. Dimopoulos, P.; Raus, T.; Bergmeier, E.; Constantinidis, T.; Iatrou, G.; Kokkini, S.; Strid, A.; Tzanoudakis, D. *Vascular Plants of Greece: An Annotated Checklist*; Botanic Garden and Botanical Museum Berlin-Dahlem: Berlin, Germany; Hellenic Botanical Society: Athens, Greece, 2013; Englera 31. [CrossRef]
38. Raunkiaer, C. *The Life Forms of Plants and Statistical Plant Geography*; Clarendon Press: Oxford, UK, 1934.
39. Michopoulos, P.; Proutsos, N.D.; Solomou, A.D.; Bourletsikas, A.; Tsilikounas, S.; Louka, V.; Lattas, P.; Kalliris, P.; Blanos, G. Effects of restoration works on soil properties of burned forest areas. In *Recent Research on Environmental Earth Sciences, Geomorphology, Soil Science, Paleoclimate, and Karst: MedGU 2023*; Çiner, A., Turan, V., Knight, J., Candeias, C., Chenchouni, H., Khan, F., Sarıkaya, M.A., Eds.; Springer: Cham, Switzerland, 2026; pp. 197–200. [CrossRef]
40. Landon, J.R. *Booker Tropical Soil Manual: A Handbook for Soil Survey and Agricultural Land Evaluation in the Tropics and Subtropics*, 1st ed.; Longman: Harlow, UK, 1984.
41. Jones, J.B., Jr. *Laboratory Guide for Conducting Soil Tests and Plant Analysis*, 1st ed.; CRC Press: Boca Raton, FL, USA, 2001.
42. Liang, K.-Y.; Zeger, S.L. Longitudinal data analysis using generalized linear models. *Biometrika* **1986**, *73*, 13–22. [CrossRef]
43. Jolliffe, I.T.; Cadima, J. Principal component analysis: A review and recent developments. *Philos. Trans. R. Soc. A Math. Phys. Eng. Sci.* **2016**, *374*, 20150202. [CrossRef] [PubMed]
44. Anderson, M.J. A new method for non-parametric multivariate analysis of variance. *Austral Ecol.* **2001**, *26*, 32–46. [CrossRef]
45. Mancl, L.A.; DeRouen, T.A. A covariance estimator for GEE with improved small-sample properties. *Biometrics* **2001**, *57*, 126–134. [CrossRef] [PubMed]
46. Leverkus, A.B.; Lorite, J.; Navarro, F.B.; Sánchez-Cañete, E.P.; Castro, J. Post-fire salvage logging alters species composition and reduces cover, richness, and diversity in Mediterranean plant communities. *J. Environ. Manag.* **2014**, *133*, 323–331. [CrossRef] [PubMed]
47. Fay, M.P.; Graubard, B.I. Small-sample adjustments for Wald-type tests using sandwich estimators. *Biometrics* **2001**, *57*, 1198–1206. [CrossRef] [PubMed]
48. Wang, M.; Long, Q. Modified robust variance estimator for generalized estimating equations with improved small-sample performance. *Stat. Med.* **2011**, *30*, 1278–1291. [CrossRef] [PubMed]

49. López-Vicente, M.; Cerdà, A.; Kramer, H.; Keesstra, S.D. Post-fire practices benefits on vegetation recovery and soil conservation in a Mediterranean area. *Land Use Policy* **2021**, *111*, 105776. [CrossRef]
50. Carrari, E.; Biagini, P.; Selvi, F. Early vegetation recovery of a burned Mediterranean forest in relation to post-fire management strategies. *Forestry* **2022**, *95*, 548–561. [CrossRef]
51. Jalali, M.; Moradi, A. Measuring and simulating pH buffer capacity of calcareous soils using empirical and mechanistic models. *Arch. Agron. Soil Sci.* **2020**, *66*, 559–571. [CrossRef]
52. Bodí, M.B.; Martin, D.A.; Balfour, V.N.; Santín, C.; Doerr, S.H.; Pereira, P.; Cerdà, A.; Mataix-Solera, J. Wildland fire ash: Production, composition and eco-hydro-geomorphic effects. *Earth-Sci. Rev.* **2014**, *130*, 103–127. [CrossRef]
53. Pereira, P.; Úbeda, X.; Martin, D.A.; Mataix-Solera, J.; Cerdà, A.; Burguet, M. Wildfire effects on extractable elements in ash from a *Pinus pinaster* forest in Portugal. *Hydrol. Process.* **2014**, *28*, 3681–3690. [CrossRef]
54. Poesen, J.; Torri, D.; Bunte, K. Effects of rock fragments on soil erosion by water at different spatial scales: A review. *Catena* **1994**, *23*, 141–166. [CrossRef]
55. Poesen, J.; Lavee, H. Rock fragments in top soils: Significance and processes. *Catena* **1994**, *23*, 1–28. [CrossRef]
56. Cerdà, A. Effects of rock fragment cover on soil infiltration, interrill runoff and erosion. *Eur. J. Soil Sci.* **2001**, *52*, 59–68. [CrossRef]
57. Pausas, J.G.; Bradstock, R.A.; Keith, D.A.; Keeley, J.E. Plant functional traits in relation to fire in crown-fire ecosystems. *Ecology* **2004**, *85*, 1085–1100. [CrossRef]
58. Keeley, J.E.; Pausas, J.G.; Rundel, P.W.; Bond, W.J.; Bradstock, R.A. Fire as an evolutionary pressure shaping plant traits. *Trends Plant Sci.* **2011**, *16*, 406–411. [CrossRef] [PubMed]
59. Paula, S.; Pausas, J.G. Burning seeds: Germinative response to heat treatments in relation to resprouting ability. *J. Ecol.* **2008**, *96*, 543–552. [CrossRef]
60. Pausas, J.G.; Verdú, M. Plant persistence traits in fire-prone ecosystems of the Mediterranean Basin: A phylogenetic approach. *Oikos* **2005**, *109*, 196–202. [CrossRef]
61. Moreira, F.; Arianoutsou, M.; Corona, P.; de las Heras, J. (Eds.) *Post-Fire Management and Restoration of Southern European Forests*; Springer: Dordrecht, The Netherlands, 2012. [CrossRef]
62. Vallejo, V.R.; Arianoutsou, M.; Moreira, F. Fire ecology and post-fire restoration approaches in southern European forest types. In *Post-Fire Management and Restoration of Southern European Forests*; Moreira, F., Arianoutsou, M., Corona, P., de las Heras, J., Eds.; Springer: Dordrecht, The Netherlands, 2012; pp. 93–119. [CrossRef]
63. Naveh, Z. The evolutionary significance of fire in the Mediterranean region. *Vegetatio* **1975**, *29*, 199–208. [CrossRef]
64. Fernández, C.; Vega, J.A.; Fonturbel, T.; Barreiro, A.; Lombao, A.; Gómez-Rey, M.X.; Díaz-Raviña, M.; González-Prieto, S. Effects of straw mulching on initial post-fire vegetation recovery. *Ecol. Eng.* **2016**, *95*, 138–142. [CrossRef]
65. Prats, S.A.; Martins, M.A.S.; Malvar, M.C.; Ben-Hur, M.; Keizer, J.J. Polyacrylamide application versus forest residue mulching for reducing post-fire runoff and soil erosion. *Sci. Total Environ.* **2014**, *468-469*, 464–474. [CrossRef] [PubMed]
66. Prats, S.A.; González-Pelayo, Ó.; Silva, F.C.; Bokhorst, K.J.; Baartman, J.E.M.; Keizer, J.J. Post-fire soil erosion mitigation at the scale of swales using forest logging residues at a reduced application rate. *Earth Surf. Process. Landf.* **2019**, *44*, 2837–2848. [CrossRef]
67. Doerr, S.H.; Shakesby, R.A.; Walsh, R.P.D. Soil water repellency: Its causes, characteristics and hydro-geomorphological significance. *Earth-Sci. Rev.* **2000**, *51*, 33–65. [CrossRef]
68. DeBano, L.F. The role of fire and soil heating on water repellency in wildland environments: A review. *J. Hydrol.* **2000**, *231-232*, 195–206. [CrossRef]
69. Santín, C.; Doerr, S.H. Fire effects on soils: The human dimension. *Philos. Trans. R. Soc. B Biol. Sci.* **2016**, *371*, 20150171. [CrossRef] [PubMed]
70. Caon, L.; Vallejo, V.R.; Ritsema, C.J.; Geissen, V. Effects of wildfire on soil nutrients in Mediterranean ecosystems. *Earth-Sci. Rev.* **2014**, *139*, 47–58. [CrossRef]